

Reductive amination of carboxylic acids under H₂ using a heterogeneous Pt–Mo catalyst

Katsumasa Sakoda,^a Sho Yamaguchi,^{a,b} Kazuki Honjo,^a Yasutaka Kitagawa,^{a,b,c,d,e}

Takato Mitsudome^{a,b,f} and Tomoo Mizugaki^{*a,b,c}

*Corresponding author: mizugaki.tomoo.es@osaka-u.ac.jp

^a Department of Materials Engineering Science, Graduate School of Engineering Science, Osaka University, 1-3 Machikaneyama, Toyonaka, Osaka 560-8531, Japan

^b Innovative Catalysis Science Division, Institute for Open and Transdisciplinary Research Initiatives (ICS-OTRI), Osaka University, Suita, Osaka 565-0871, Japan

^c Research Center for Solar Energy Chemistry, Graduate School of Engineering Science, Osaka University, 1-3 Machikaneyama, Toyonaka, Osaka 560-8531, Japan

^d Center for Quantum Information and Quantum Biology (QIQB), Osaka University, Toyonaka, Osaka 560-8531, Japan

^e Spintronics Research Network Division, Institute for Open and Transdisciplinary Research Initiatives (SRN-OTRI), Osaka University, Toyonaka, Osaka 560-8531, Japan

^f PRESTO, Japan Science and Technology Agency (JST), 4-1-8 Honcho, Kawaguchi, Saitama 333-0012, Japan

Table of Content

1. General experimental details	S3
2. Catalyst preparation and reaction procedures	S4
3. Supplementary tables	S7
Table S1 Investigation of catalyst preparation methods	S7
Table S2 Investigation of pre-reduction effect.....	S7
Table S3 Investigation of support effect	S8
Table S4 SSA _{BET} and acidity of Pt–Mo catalysts	S9
Table S5 Reusability of Pt–Mo/ γ -Al ₂ O ₃ and Pt–Mo/TiO ₂ for the reductive amination.....	S10
Table S6 ICP-AES and CHN analyses of fresh, 1st used, and 6th used Pt–Mo/ γ -Al ₂ O ₃	S11
Table S7 EDX analyses of fresh, 1st used, and 6th used Pt–Mo/ γ -Al ₂ O ₃ and Pt–Mo/TiO ₂	S11
Table S8 Previously reported catalysts for the reductive amination of carboxylic acids under H ₂	S12
Table S9 Detailed product analysis of the substrate scope of carboxylic acids with 1a	S13
Table S10 Detailed product analysis of the substrate scope of amines with 2a	S14
4. Supplementary figures	S15
Fig. S1 (a) NH ₃ -TPD profiles of Pt–Mo/Support. Relationship between the yields of 3a and (b) weak, (c) strong, and (d) total acid densities measured by NH ₃ -TPD. Relationship between the yields of 3a and (e) weak, (f) strong, and (g) total acid density amounts measured by NH ₃ -TPD. NH ₃ desorption was monitored by mass number $m/z = 16$ during heating.	S15
Fig. S2 XPS spectra in the Pt 4d _{5/2} region of Pt–Mo/ γ -Al ₂ O ₃ , Pt–Mo/TiO ₂ , Pt–Mo/Nb ₂ O ₅ , Pt–Mo/SiO ₂ , and Pt/ γ -Al ₂ O ₃	S16
Fig. S3 FT-IR spectra of fresh, 1st used, and 6th used Pt–Mo/ γ -Al ₂ O ₃	S17
Fig. S4 Linear combination fitting analysis of Mo K-edge XANES spectrum of reduced Pt–Mo/ γ -Al ₂ O ₃	S17
Fig. S5 Time-course data of the Pt–Mo/ γ -Al ₂ O ₃ catalyzed reductive amination of 2a with 1a to 3a . Product distribution was determined based on (a) 1a and (b) 2a	S18
Fig. S6 (a) <i>In situ</i> pyridine adsorption FT-IR analysis of Pt–Mo/ γ -Al ₂ O ₃ , and Pt/ γ -Al ₂ O ₃ , and (b) NH ₃ -TPD profiles for Pt–M/ γ -Al ₂ O ₃ (M = Mo, Re, W, or V) and Pt/ γ -Al ₂ O ₃ . Acid amount is presented in parentheses.	S18
Fig. S7 Illustration of (a) model A and (b) model B	S19
5. Supplementary schemes	S22
Scheme S1 Control experiments. (a) Hydrogenation of 4b . (b) Amination of 1-propanol with 1a . (c) Reductive amination of propionaldehyde with 1a	S22
Scheme S2 Proposed major reaction path for the reductive amination of 2a with 1a over a Pt–Mo/ γ -Al ₂ O ₃	S23
6. Product identification	S24
7. References	S40

1. General experimental details

Organic chemicals were purchased from Fujifilm Wako Pure Chemical Industries, Ltd., Tokyo Chemical Industry Co., Ltd., and Sigma-Aldrich and were used as received. H_2PtCl_6 , RuCl_3 , K_3RhCl_6 , and $\text{Pd}(\text{NH}_3)_4\text{Cl}_2$ hydrates were obtained from N. E. Chemcat. $(\text{NH}_4)_6\text{Mo}_7\text{O}_{24}\cdot 4\text{H}_2\text{O}$, NH_4VO_3 , $(\text{NH}_4)_{10}(\text{H}_2\text{W}_{12}\text{O}_{42})\cdot 4\text{H}_2\text{O}$, and NaReO_4 were purchased from Nacalai Tesque, Kishida Chemical, Sigma-Aldrich, and Alfa Aesar Co., Ltd., respectively. $\gamma\text{-Al}_2\text{O}_3$ was obtained from Sumitomo Chemical Co., Ltd. $\alpha\text{-Al}_2\text{O}_3$ and WO_3 were purchased from Fujifilm Wako Pure Chemical Industries, Ltd. TiO_2 (JRC-TIO-2), Nb_2O_5 (JRC-NBO-2), ZrO_2 (JRC-ZRO-7), and CeO_2 (JRC-CEO-2) were supplied by the Catalyst Society of Japan as reference catalysts. SiO_2 (CARiACT, Q-6) was purchased from Fuji Silysia Chemical, Ltd. Gas chromatography (GC-FID) analyses were performed on a Shimadzu GC-2014 instrument equipped with a capillary column (InertCap for amines, GL Science, 30 m \times 0.32 mm i.d.). Gas chromatography-mass spectrometry (GC-MS) analyses were performed on a Shimadzu QP-2010SE instrument equipped with a capillary column (SH-Rtx-200MS, Shimadzu, 30 m \times 0.25 mm i.d. film thickness 0.25 μm). ^1H and ^{13}C nuclear magnetic resonance (NMR) spectra were recorded using a JEOL JNM-ESC400 spectrometer. Chemical shifts are reported as follows: 1,4-dioxane (3.76 ppm for ^1H NMR, 67.15 ppm for ^{13}C NMR) as an external standard in D_2O solvent, TMS (0 ppm for ^1H NMR), CDCl_3 (77.1 ppm for ^{13}C NMR). NMR multiplicities are reported using the following abbreviations: s, singlet; d, doublet; t, triplet; q, quartet; m, multiplet; br, broad; J , coupling constants in hertz. The transmission electron microscopy images were obtained using a FEI Titan Cubed G2 60-300 or FEI Tecnai G2 20ST. Scanning transmission electron microscopy images with elemental maps were collected using a FEI Titan Cubed G2 60-300 instrument, operated at 300 kV, and equipped with a Super-X energy-dispersive X-ray spectroscopy (EDX) detector. Pt L_3 -edge and Mo K-edge X-ray absorption spectra were recorded at room temperature in transmittance mode using Si (311) monochromators for the Pt L_3 -edge and Mo K-edge at the 14B2 and 01B1 beam line stations at SPring-8, Japan Atomic Energy Research Institute (JASRI), Harima, Japan (promotion numbers: 2021B1945, 2022B1699, 2022B0519, and 2022B0586). Data analysis was performed using Demeter ver. 0.9.21. X-ray photoelectron spectroscopy (XPS) spectra of the samples were obtained using a ULVAC-PHI ESCA 3057 system, and the binding energy was referenced to the C 1s peak (285.0 eV). EDX measurements were performed using a Shimadzu EDX-7200 instrument. Inductively coupled plasma-atomic emission spectroscopy (ICP-AES) measurements were performed using a Perkin Elmer Optima 8300 instrument. CHN elemental analyses were performed using a Perkin Elmer 2400II CHNS/O. Fourier-transform infrared (FT-IR) spectra were recorded using a JASCO FT-IR 4100 spectrometer equipped with a mercury cadmium telluride detector. The CO adsorption, the single-point Brunauer–Emmett–Teller (BET), and the NH_3 -temperature programmed desorption (TPD) data were measured using a BELCAT-A instrument (BEL Japan Inc.) equipped with a thermal conductivity detector or mass spectrometer (BELMASSII, BEL Japan Inc.).

2. Catalyst preparation and reaction procedures

Preparation of metal oxide-supported Pt–Mo catalysts

The Pt–Mo/ γ -Al₂O₃ catalyst was prepared using a co-impregnation method. An aqueous solution of H₂PtCl₆ (6.00 mL, 100 mM), (NH₄)₆Mo₇O₂₄·4H₂O (2.00 mL, 75 mM) and γ -Al₂O₃ (1.000 g) were added to distilled water (50 mL) at room temperature. After stirring for 12 h in air, water was removed by rotary evaporation under reduced pressure to obtain the solid product. The obtained powder was dried at 110 °C for 5 h. After drying, the product was calcined at 500 °C for 3 h under a static air atmosphere to obtain Pt–Mo/ γ -Al₂O₃ as a black powder. As determined using ICP-AES, the Pt and Mo contents in Pt–Mo/ γ -Al₂O₃ were 9.78 and 1.41 wt%, respectively. The other catalysts were prepared in a similar way using various metal salts and supports. All catalysts were applied to the reaction without any pre-reduction step.

Preparation of Pt/Mo/ γ -Al₂O₃ and Mo/Pt/ γ -Al₂O₃ catalysts (Table S1)

The Pt/Mo/ γ -Al₂O₃ and Mo/Pt/ γ -Al₂O₃ catalysts were prepared using a sequential impregnation method. An aqueous solution of (NH₄)₆Mo₇O₂₄·4H₂O (2.00 mL, 75 mM) and γ -Al₂O₃ (1.000 g) were added to distilled water (50 mL) at room temperature. After stirring for 12 h in air, water was removed by rotary evaporation under reduced pressure to obtain the solid product. The obtained powder was dried at 110 °C for 5 h. After drying, the product and an aqueous solution of H₂PtCl₆ (6.00 mL, 100 mM) were added to distilled water (50 mL) at room temperature and stirred for 12 h. Then, water was removed by rotary evaporation and the product was dried at 110 °C for 5 h. Finally, the obtained powder was calcined at 500 °C for 3 h under a static air atmosphere to obtain Pt/Mo/ γ -Al₂O₃ as a black powder. The Mo/Pt/ γ -Al₂O₃ catalyst were prepared in a similar way, changing the order of Pt and Mo precursor additions.

Typical reductive amination procedure (Table 1, entry 1)

The reductive amination of acetic acid (**2a**) with piperidine (**1a**) was carried out in a 50 mL stainless steel autoclave equipped with a Teflon vessel. The vessel was charged with **1a** (0.085 g, 1.0 mmol), **2a** (0.180 g, 3.0 mmol), Pt–Mo/ γ -Al₂O₃ (0.150 g), *n*-hexane (3 mL), and a Teflon-coated magnetic stir bar was added. The reactor was sealed, purged five times with 1.0 MPa H₂, and then pressurized (2.0 MPa), heated to 100 °C, and stirred at 900 rpm for 12 h. After the reaction, the autoclave was cooled in an ice-water bath, and H₂ gas was released. The resulting reaction mixture was diluted with 1-butanol and analyzed by GC-FID. Product yields were calculated based on **1a**.

Catalyst reuse experiments (Fig. 1 and Table S5)

After the reductive amination was complete, the catalyst was separated from the reaction mixture by centrifugation, washed with ethanol and *n*-hexane in air before being reused in a subsequent reaction.

Reductive amination under atmospheric H₂ pressure (Scheme 2a)

The reductive amination under atmospheric H₂ pressure was carried out in a Schlenk tube equipped with a balloon and condenser. The Schlenk tube was charged with **1a** (0.085 g, 1.0 mmol), **2a** (0.180 g, 3.0 mmol), Pt–Mo/γ-Al₂O₃ (0.150 g), *n*-dodecane (3 mL), and a Teflon-coated magnetic stir bar was added. The reaction mixture was degassed twice by the freeze-pump-thaw method, filled with 0.1 MPa H₂, heated to 140 °C, and stirred at 900 rpm for 24 h. After the reaction, the reactor was cooled, and H₂ gas was released. The resulting reaction mixture was diluted with 1-butanol and analyzed by GC-FID.

Gram-scale reaction (Scheme 2b)

The gram-scale reductive amination was carried out in a 100 mL stainless steel autoclave equipped with a Teflon vessel. The vessel was charged with **1a** (1.00 g, 11.7 mmol), **2a** (2.00 g, 33.3 mmol), Pt–Mo/γ-Al₂O₃ (0.150 g), *n*-hexane (10 mL), and a Teflon-coated magnetic stir bar was added. The reactor was purged five times with 1.0 MPa H₂ and then pressurized to 4.0 MPa at room temperature, heated to 160 °C, and stirred at 1000 rpm for 48 h. After the reaction, the autoclave was cooled in an ice-water bath, and the H₂ gas was carefully released. Pt–Mo/γ-Al₂O₃ was separated by filtration, and hydrogen chloride solution (1.25 M, 1,4-dioxane) was added. The solvents were evaporated, washed with diethyl ether and water, then the water phase was gathered, evaporated, and dried to give pure hydrogen chloride salt **3a** (1.64 g, 10.9 mmol, 93%).

TON based on surface Pt atoms was described by the following equation:

$$TON = \frac{\text{mole of product}}{W_{\text{catalyst}} \times \frac{\text{Pt loading}}{\text{atomic weight of Pt}} \times \text{dispersion}} \quad (\text{eq. S1})$$

W_{catalyst} : the gram of catalyst used in the reductive amination

Pt loading: the loading amount of Pt measured by ICP-AES analysis (Table S6)

dispersion: Pt dispersion measured by CO pulse chemisorption analysis (40.2%)

Pt–Mo/γ-Al₂O₃ pre-reduction (Fig. 2 and S3, and Table S2)

Pt–Mo/γ-Al₂O₃ is pre-reduced for characterizations in Fig. 2 and S3, and control experiment in Table S2 under the typical reductive amination condition without substrates: Pt–Mo/γ-Al₂O₃ (0.150 g), *n*-hexane (3 mL), 100 °C, H₂ (2.0 MPa), 2 h.

Synthesis of *N*-propionylpiperidine (**4b**)

4b was prepared according to literature procedures.^{S1} The Schlenk tube was charged with **1a** (2.00 g, 23.5 mmol), propionyl chloride (1.00 g, 10.8 mmol), and CHCl₃ (10 mL) in an ice-water bath, and a Teflon-coated magnetic stir bar was added. The reactor was heated to 80 °C, and stirred at 900 rpm for 2 h. After the reaction, the solvents were evaporated, washed with diethyl ether and water, then the organic phase was gathered, evaporated, and distilled to give pure **4b** (0.827 g, 5.87 mmol, 54%).

3. Supplementary tables

The influence of catalyst preparation method and H₂ pre-reduction was investigated. Pt/Mo/ γ -Al₂O₃ and Mo/Pt/ γ -Al₂O₃ prepared by the sequential impregnation method showed almost the same yields as that of co-impregnated Pt–Mo/ γ -Al₂O₃ under the typical reductive amination conditions (Table S1 entries 2 and 3 vs. entry 1). Pt–Mo/ γ -Al₂O₃ pre-reduced under 2 MPa H₂ for 2 h at 100 °C provided **3a** in 27% and 97% yield after 2 and 12 h, respectively. This result is comparable to that of untreated Pt–Mo/ γ -Al₂O₃ (Table S2, entries 3 and 4 vs. entries 1 and 2), indicating that the Pt and Mo species are easily reduced under the reaction conditions to form the active Pt and Mo species.

Table S1 Investigation of catalyst preparation methods^a

entry	catalyst	conv. of 1a ^b [%]	yield ^b [%]	
			3a	4a
1	Pt–Mo/ γ -Al ₂ O ₃	>99	98	0
2	Pt/Mo/ γ -Al ₂ O ₃	>99	95	0
3	Mo/Pt/ γ -Al ₂ O ₃	>99	94	0

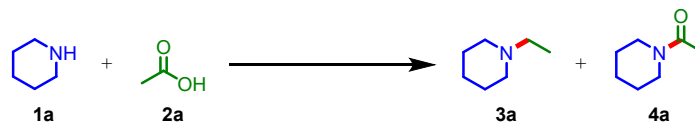
^a Reaction conditions: Pt–Mo catalyst (0.15 g, Pt: 8 mol% and Mo: 2 mol%), **1a** (1 mmol), **2a** (3 mmol), *n*-hexane (3 mL), 100 °C, H₂ (2 MPa), 12 h.

^b Conversion and yield were determined by GC-FID using an internal standard.

Table S2 Investigation of pre-reduction effect^a

entry	catalyst	reaction time (h)	conv. of 1a ^b [%]	yield ^b [%]	
				3a	4a
1	Pt–Mo/ γ -Al ₂ O ₃	2	29	28	0
2	Pt–Mo/ γ -Al ₂ O ₃	12	>99	98	0
3	reduced Pt–Mo/ γ -Al ₂ O ₃ ^c	2	27	27	0
4	reduced Pt–Mo/ γ -Al ₂ O ₃ ^c	12	>99	97	0

^a Reaction conditions: Pt–Mo/ γ -Al₂O₃ (0.15 g, Pt: 8 mol% and Mo: 2 mol%), **1a** (1 mmol), **2a** (3 mmol), *n*-hexane (3 mL), 100 °C, H₂ (2 MPa). ^b Conversion and yield were determined by GC-FID using an internal standard. ^c Pre-reduction was performed under 2 MPa of H₂ at 100 °C for 2 h.

Table S3 Investigation of support effect^a

catalyst	loading amount ^b [wt%]		conv. of 1a ^c [%]	yield ^c [%]		selectivity of 3a [%]	TON ^d
	Pt	Mo		3a	4a		
Pt–Mo/ γ -Al ₂ O ₃	10.3	1.28	29	28	0	97	3.5
Pt–Mo/ α -Al ₂ O ₃	6.93	1.05	22	18	<1	82	3.4
Pt–Mo/TiO ₂	7.25	1.29	26	26	0	>99	4.7
Pt–Mo/Nb ₂ O ₅	9.24	1.36	30	22	0	73	3.1
Pt–Mo/WO ₃	8.09	1.09	25	22	<1	88	3.5
Pt–Mo/ZrO ₂	8.12	- ^e	26	20	0	77	3.2
Pt–Mo/CeO ₂	9.91	1.13	59	6	0	10	0.8
Pt–Mo/SiO ₂	8.08	1.13	18	5	0	28	0.8

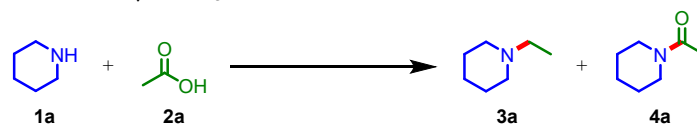
^a Reaction conditions: Pt–Mo catalyst (0.15 g), **1a** (1 mmol), **2a** (3 mmol), *n*-hexane (3 mL), 100 °C, H₂ (2 MPa), 2 h.

^b Loading amounts of Pt and Mo were measured by EDX. ^c Conversion and yield were determined by GC-FID using an internal standard. ^d TON was calculated based on total Pt atoms. ^e The Mo loading amount in Pt–Mo/ZrO₂ could not be determined because the characteristic X-rays of Mo K- α and Zr K- β are overlapped.

Table S4 SSA_{BET} and acidity of Pt–Mo catalysts

sample	SAA _{BET} ^a (m ² /g)	acidity ^b (μmol/g)			acid density ^c (μmol/m ²)			acid amount ^d (μmol)		
		weak	strong	total	weak	strong	total	weak	strong	total
Pt–Mo/γ-Al ₂ O ₃	120.9	84.7	43.0	127.7	0.7	0.4	1.1	12.7	6.4	19.2
Pt–Mo/α-Al ₂ O ₃	15.9	11.6	6.9	18.5	0.7	0.4	1.1	1.7	1.0	2.7
Pt–Mo/TiO ₂	22.1	13.6	15.0	28.6	0.6	0.7	1.3	2.0	2.3	4.3
Pt–Mo/Nb ₂ O ₅	9.2	5.3	7.4	12.7	0.6	0.8	1.4	0.8	1.1	1.9
Pt–Mo/WO ₃	13.1	5.5	9.8	15.3	0.4	0.8	1.2	0.8	1.5	2.3
Pt–Mo/ZrO ₂	26.8	14.6	18.1	32.7	0.5	0.7	1.2	2.2	2.7	4.9
Pt–Mo/CeO ₂	95.2	110.6	29.0	139.6	1.2	0.3	1.5	16.6	4.4	21.0
Pt–Mo/SiO ₂	433.9	73.0	0.0	73.0	0.2	0.0	0.2	11.0	0.0	11.0
Pt/γ-Al ₂ O ₃	131.8	121.6	36.9	158.5	0.9	0.3	1.2	18.2	5.5	23.7
Mo/γ-Al ₂ O ₃	138.9	146.3	25.5	171.8	1.1	0.2	1.3	21.9	3.8	25.7
γ-Al ₂ O ₃	154.8	116.9	69.2	186.1	0.8	0.4	1.2	17.5	10.4	27.9

^a Measured by the single-point BET method. ^b Measured by NH₃-TPD. ^c Calculated based on “acidity (μmol/g)” / “SSA_{BET} (m²/g)”. ^d Acid amount in the reaction system calculated based on “acidity (μmol/g)” × “The weight of catalyst used (0.150 g)”.

Table S5 Reusability of Pt–Mo/ γ -Al₂O₃ and Pt–Mo/TiO₂ for the reductive amination^a

entry	catalyst	run	conv. of 1a ^b [%]	yield ^b [%]		TON ^c	total TON
				3a	4a		
1	Pt–Mo/ γ -Al ₂ O ₃	1st	>99	97	1	12	70
2		2nd	>99	97	1	12	
3		3rd	93	92	1	12	
4		4th	91	90	1	11	
5		5th	94	93	1	12	
6		6th	86	85	1	11	
7	Pt–Mo/TiO ₂	1st	>99	>99	0	18	45
8		2nd	42	42	0	8	
9		3rd	34	34	0	6	
10		4th	39	35	0	6	
11		5th	33	25	0	4	
12		6th	20	18	0	3	

^a Reaction conditions: Pt–Mo catalyst (0.15 g), **1a** (1 mmol), **2a** (3 mmol), *n*-hexane (3 mL), 100 °C, H₂ (2 MPa), 12 h. ^b Conversion and yield were determined by GC-FID using an internal standard. ^c Based on total Pt atoms measured by EDX (Pt–Mo/ γ -Al₂O₃: 10.3 wt%, Pt–Mo/TiO₂: 7.25 wt%).

The reason for the deactivation of Pt–Mo catalysts was investigated. Inductively coupled plasma-atomic emission spectroscopy analysis of the Pt–Mo/ γ -Al₂O₃ catalyst after the 1st and 6th runs showed that the metal contents decrease compared to those of the fresh catalyst (Table S6). CHN analysis revealed an increase in the C and H contents before and after the reaction, indicating accumulation of organic species on the catalyst surface (see Fig. S3 for details). To exclude the influence of adsorbed species, the Pt/Al, Mo/Al, and Mo/Pt atomic ratios of Pt–Mo/ γ -Al₂O₃ were calculated. The atomic ratio of Pt/Al was almost constant even after 6th run, indicating leaching of Pt species is negligible. Regarding the Mo/Al and Mo/Pt atomic ratios, the fresh catalyst and that after the 1st run showed similar ratio, while that after the 6th run exhibited lower values. We also examined the EDX measurement of Pt–Mo/TiO₂, and the Mo/Ti and Mo/Pt atomic ratios were significantly decreased even after the 1st run compared to that of fresh catalyst (Table S7). These results clearly show that γ -Al₂O₃ support effectively suppress the leaching of Mo species into the reaction mixture during the reductive amination.

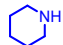
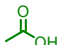
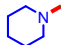
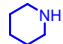
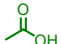
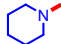
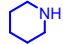
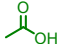
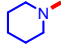
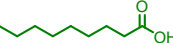
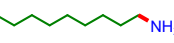
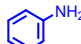
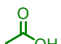
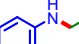
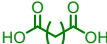
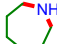
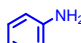
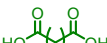
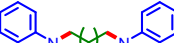

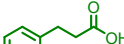
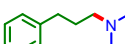
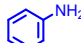
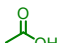
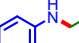
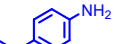
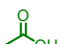
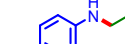
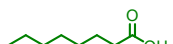
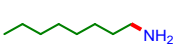
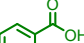
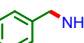
Table S6 ICP-AES and CHN analyses of fresh, 1st used, and 6th used Pt–Mo/ γ -Al₂O₃

sample	amount [wt%]						atomic ratio		
	Pt	Mo	Al	C	H	N	Pt/Al	Mo/Al	Mo/Pt
fresh Pt–Mo/ γ -Al ₂ O ₃	10.1	1.42	42.0	0.05	0.47	0.08	0.033	0.010	0.29
1st used Pt–Mo/ γ -Al ₂ O ₃	9.67	1.30	38.7	4.13	0.80	0.14	0.035	0.010	0.27
6th used Pt–Mo/ γ -Al ₂ O ₃	5.89	0.42	28.0	15.66	2.23	0.13	0.029	0.004	0.15

Table S7 EDX analyses of fresh, 1st used, and 6th used Pt–Mo/ γ -Al₂O₃ and Pt–Mo/TiO₂

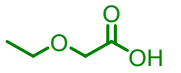
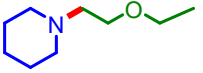
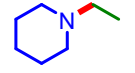
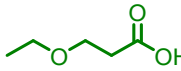
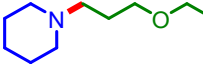
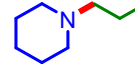
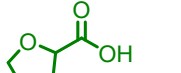
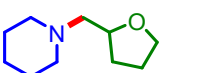
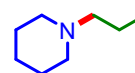
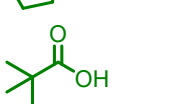
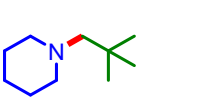
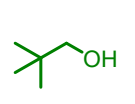
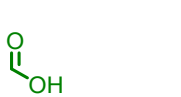

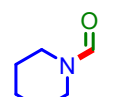

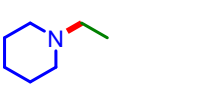
sample	atomic ratio				
	Pt/Al	Mo/Al	Pt/Ti	Mo/Ti	Mo/Pt
fresh Pt–Mo/ γ -Al ₂ O ₃	0.041	0.011	-	-	0.26
1st used Pt–Mo/ γ -Al ₂ O ₃	0.041	0.011	-	-	0.25
6th used Pt–Mo/ γ -Al ₂ O ₃	0.042	0.006	-	-	0.14
fresh Pt–Mo/TiO ₂	-	-	0.034	0.014	0.40
1st used Pt–Mo/TiO ₂	-	-	0.036	0.010	0.29
6th used Pt–Mo/TiO ₂	-	-	0.034	0.006	0.16

Table S8 Previously reported catalysts for the reductive amination of carboxylic acids under H₂

catalyst	amine	carboxylic acid	product	reaction conditions	TON ^a	ref.
Pt–Mo/ γ -Al ₂ O ₃				<i>n</i> -hexane, 2 MPa H ₂ 100 °C, 12 h	13 (32) ^b	this work Table 1, entry 1
Pt–Mo/ γ -Al ₂ O ₃				<i>n</i> -dodecane, 0.1 MPa H ₂ 140 °C, 24 h	9 (23) ^b	this work Scheme 2a
Pt–Mo/ γ -Al ₂ O ₃				<i>n</i> -hexane, 4 MPa H ₂ 160 °C, 48 h	146 (363) ^b	this work Scheme 2b
[Ru ₂ (triphos) ₂ Cl ₃]Cl	NH ₃			THF, 4 MPa H ₂ 164 °C, 14 h	93	S2
Ru(acac) ₃ , triphos ^c , HNTf ₂ ^d				THF, 6 MPa H ₂ 160 °C, 18 h	42	S3
Ru(acac) ₃ , triphos ^c , MSA ^e	NH ₃			1,4-dioxane, 1 MPa H ₂ 220 °C, 88 h	33	S4
Ru(acac) ₃ , triphos ^c , MSA ^e				1,4-dioxane, 1 MPa H ₂ 220 °C, 42 h	49	S5
Re/TiO ₂				octane, 5 MPa H ₂ 200 °C, 48 h	41	S6
Co(BF ₄) ₂ ·6H ₂ O, L1 ^f				1,4-dioxane, 4 MPa H ₂ 100 °C, 24 h	30	S7
Co(BF ₄) ₂ ·6H ₂ O, triphos ^c				CPME ^g , 6 MPa H ₂ 140 °C, 24 h	15	S8
RuWO _x /MgAl ₂ O ₄	NH ₃			CPME ^g , 5 MPa H ₂ 200 °C, 6.5 h	16	S9
Au/TiO ₂	NH ₃			CPME ^g , 3 MPa H ₂ 200 °C, 70 h	257	S10

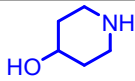
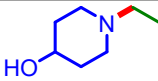
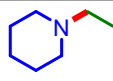
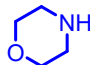
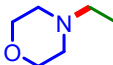
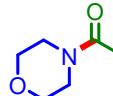
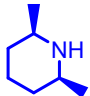
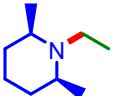
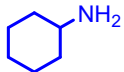
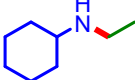
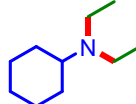
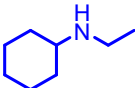
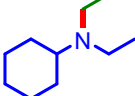
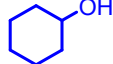
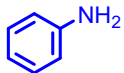
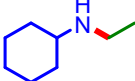
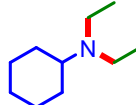
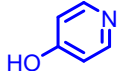
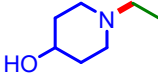
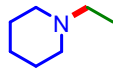
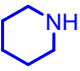
^a TON was calculated based on total metal loading. ^b Based on total Pt atoms measured by ICP-AES analysis in Table S6 (10.1 wt%); based on surface Pt atoms in parentheses. ^c (1,1,1-tris(diphenylphosphinomethyl)ethane. ^d Trifluoromethanesulfonimide. ^e Methane sulphonic acid. ^f CH₃C(CH₂PPh'₂)₃ (Ph' = *p*-anisole) ^g Cyclopentyl methyl ether.

Table S9 Detailed product analysis of the substrate scope of carboxylic acids with **1a**

carboxylic acid	conditions	conv. of 1a (%)	product and yield (%)
	2 MPa H ₂ , 140 °C, 20 h	>99	 (59)  (33)
	2 MPa H ₂ , 140 °C, 20 h	>99	 (48)  (16)
	2 MPa H ₂ , 160 °C, 30 h	>99	 (43)  (25)
	2 MPa H ₂ , 160 °C, 50 h	44	 <1  39 ^a
	2 MPa H ₂ , 100 °C, 12 h	77	 <1  71
	2 MPa H ₂ , 100 °C, 12 h	19	 <1

Conversion and yield were determined by GC-FID using an internal standard and calculated based on the **1a**. The yields in parentheses were based on ¹H NMR analysis. ^a The yield was calculated based on the carboxylic acid.

Table S10 Detailed product analysis of the substrate scope of amines with **2a**

amine	conditions	conv. of 1a (%)	product and yield (%)				
	2 MPa H ₂ , 120 °C, 24 h	>99		83		11	
	4 MPa H ₂ , 100 °C, 12 h	98		81		5	
	2 MPa H ₂ , 140 °C, 24 h	25		(7)			
	2 MPa H ₂ , 100 °C, 16 h ^a	99		90		8	
	2 MPa H ₂ , 140 °C, 24 h ^b	87		58		21	
	3 MPa H ₂ , 100 °C, 16 h ^a	>99		40		11	
	3 MPa H ₂ , 120 °C, 18 h	>99		55		18	 2

Conversion and yield were determined by GC-FID using an internal standard and calculated based on the amines. The yields in parentheses were based on ¹H NMR analysis. ^a **2a** (4 mmol). ^b **2a** (5 mmol).

4. Supplementary figures

To investigate support effect, NH₃-TPD and XPS analyses of Pt–Mo catalysts were carried out (Fig. S1). The yields of **3a** in Table S3 were plotted against the weak, strong, and total acid densities and amounts in the reaction system in Table S4, as shown in Fig. S1b–g. These data indicate that the acid densities are positively correlated with the yield of **3a**; especially, this tendency is clearly observed in the case of strong acid density (Fig. S1b–d). In the proposed mechanism as shown in Scheme S2, acid sites may promote the enamine formation from hemiaminal, i.e., step VIb. Use of the supports with high acid density enhance the number of acid sites closely located in the vicinity of Pt–Mo sites, which may contribute to the efficient reductive amination of carboxylic acids. In the XPS spectrum of Pt–Mo/ γ -Al₂O₃ in the Pt 4d_{5/2} region, a Pt 4d_{5/2} peak was observed at 315.3 eV, which is lower than that of Pt/ γ -Al₂O₃ observed at 315.8 eV (Fig. S2). The spectra of Pt–Mo/Nb₂O₅ and Pt–Mo/SiO₂ exhibited peaks at similar binding energy with Pt–Mo/ γ -Al₂O₃. In addition, the Pt 4d_{5/2} peak of Pt–Mo/TiO₂ appeared at a slightly lower binding energy of 314.6 eV. The presence of negatively charged Pt species of Pt–Mo/TiO₂ may increase H₂ activation ability of Pt nanoparticle in 1st run (Scheme S2, step II).

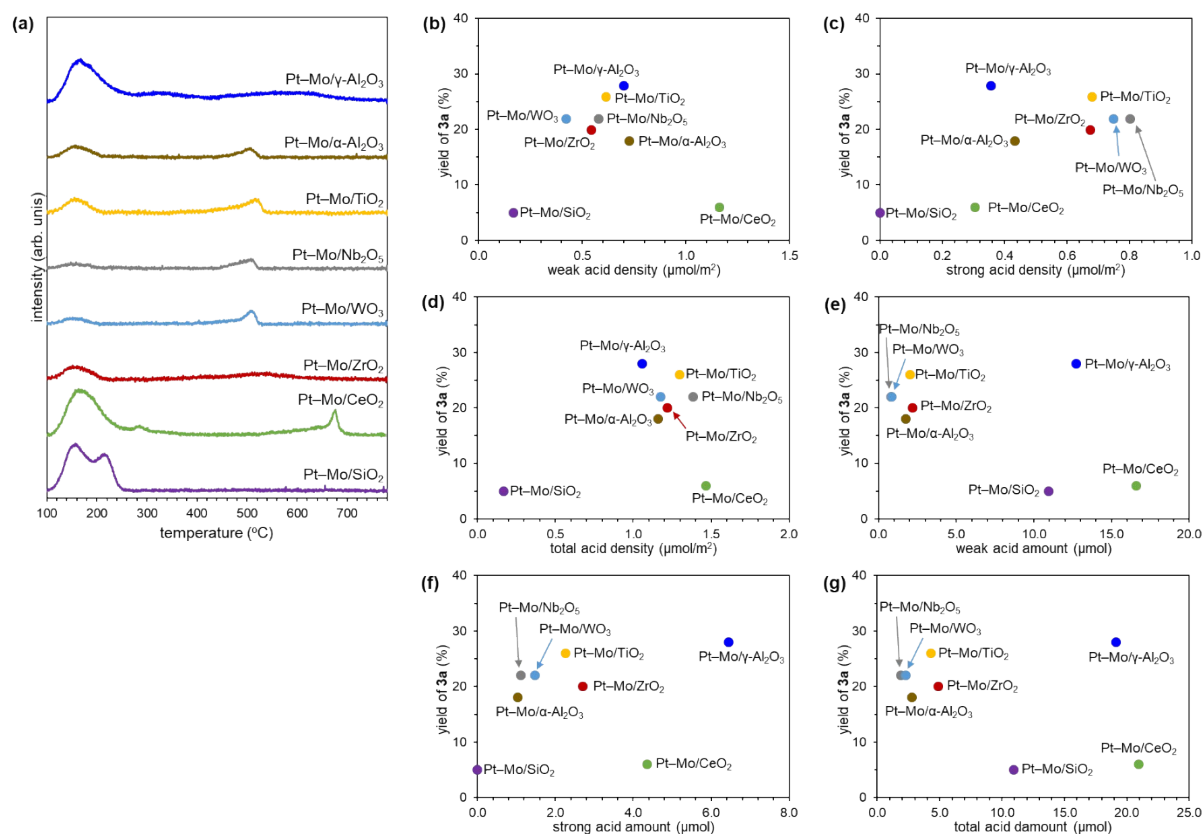


Fig. S1 (a) NH₃-TPD profiles of Pt–Mo/Support. Relationship between the yields of **3a** and (b) weak, (c) strong, and (d) total acid densities measured by NH₃-TPD. Relationship between the yields of **3a** and (e) weak, (f) strong, and (g) total acid amounts measured by NH₃-TPD. NH₃ desorption was monitored by mass number $m/z = 16$ during heating.

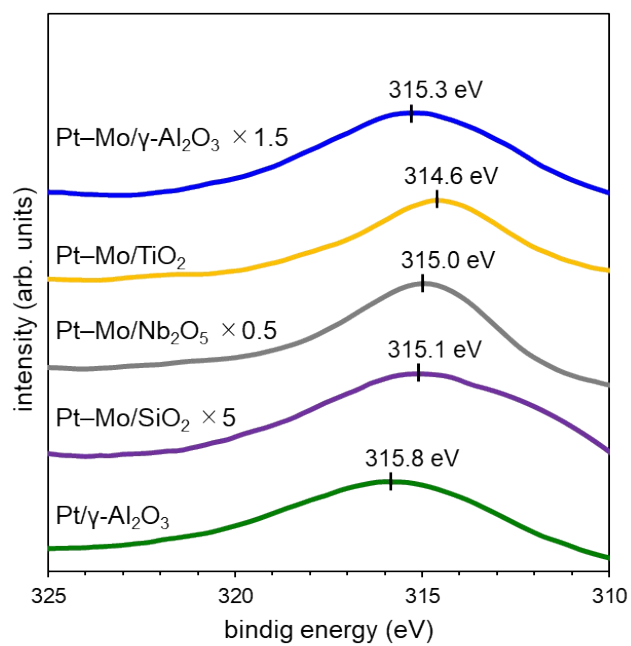


Fig. S2 XPS spectra in the Pt 4d_{5/2} region of Pt-Mo/ γ -Al₂O₃, Pt-Mo/TiO₂, Pt-Mo/Nb₂O₅, Pt-Mo/SiO₂, and Pt/ γ -Al₂O₃.

To clarify the adsorbed organics, we conducted FT-IR analysis of the used catalysts (Fig. S3). The IR spectrum of the 6th used Pt–Mo/ γ -Al₂O₃ showed two strong absorption bands at 1583 and 1476 cm⁻¹ assignable to the C–O stretching mode of the bidentate acetate species.^{S11,S12} Thus, the decreases in the apparent metal contents was caused by adsorption of bidentate acetate species.

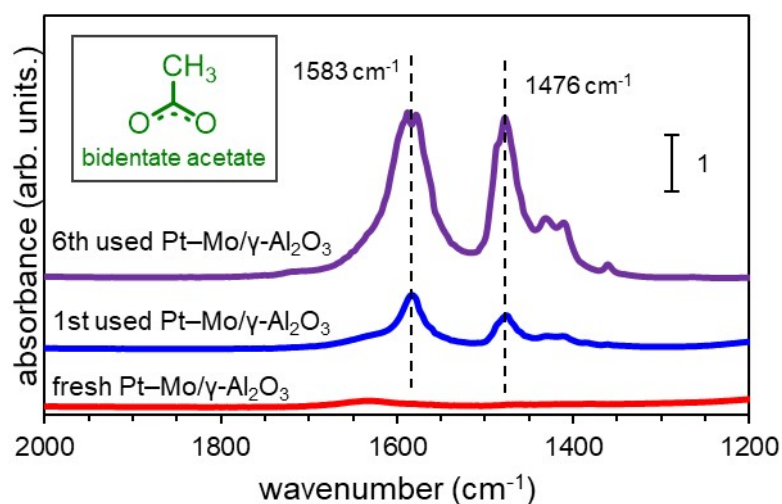


Fig. S3 FT-IR spectra of fresh, 1st used, and 6th used Pt–Mo/ γ -Al₂O₃.

Fig. S4 shows Mo K-edge XANES pattern fitting analysis of reduced Pt–Mo/ γ -Al₂O₃. Mo₂C, MoO₂ and MoO₃ were used as standards for the Mo²⁺, Mo⁴⁺, and Mo⁶⁺ oxidation states, respectively. This result indicates that the ratio of Mo²⁺, Mo⁴⁺, and Mo⁶⁺ were 42:40:18.

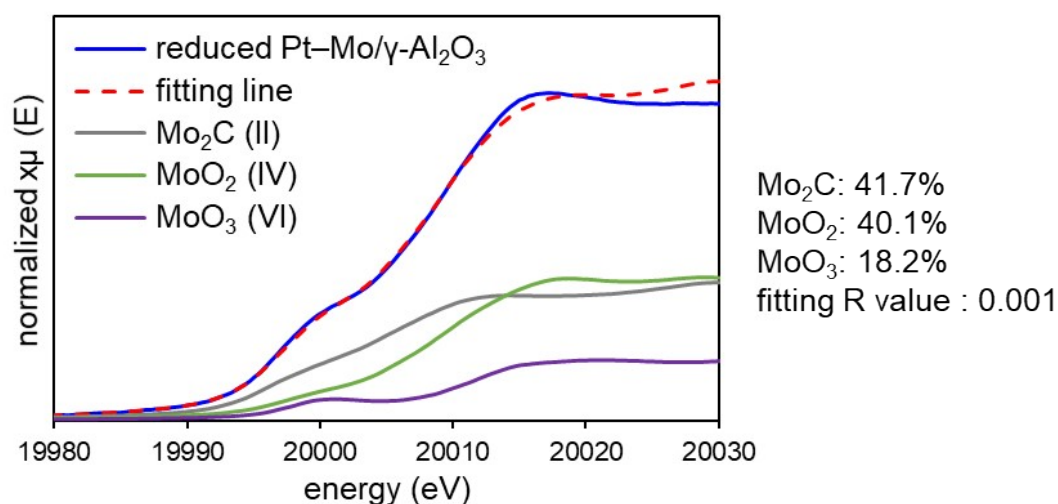


Fig. S4 Liner combination fitting analysis of Mo K-edge XANES spectrum of reduced Pt–Mo/ γ -Al₂O₃.

The time-course experiment was performed as shown in Fig. S5. If the reductive amination of **2a** with **1a** proceeds via *N*-acetylpiperidine (**4a**) or ethanol (**5a**), the yield of **4a** or **5a** should increase and then decrease as time passed. The yields of **4a** and **5a** did not show such result (Fig. S5b), which strongly supports a possibility of the reaction pathway via aldehyde.

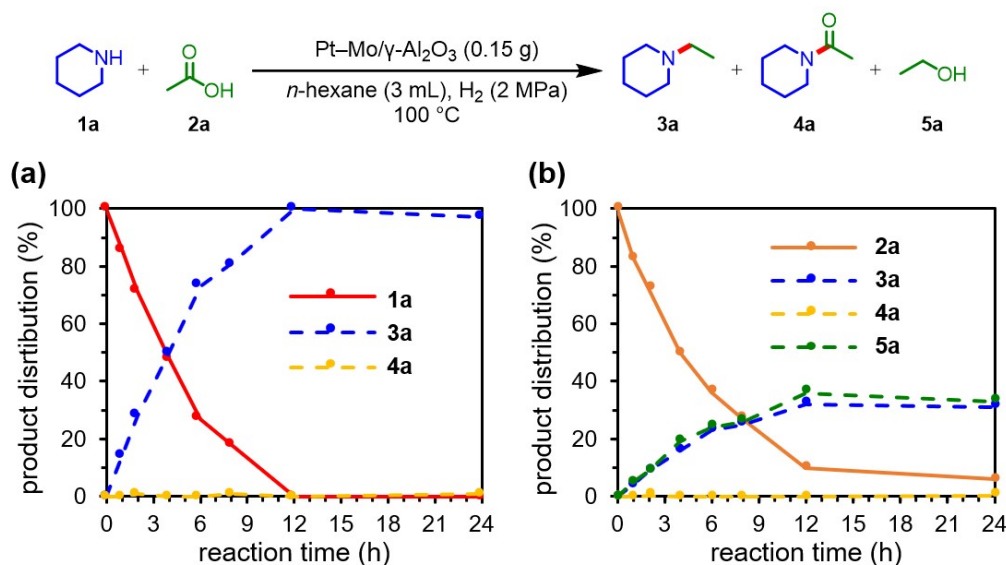


Fig. S5 Time-course data of the Pt-Mo/ γ -Al₂O₃ catalyzed reductive amination of **2a** with **1a** to **3a**. Product distribution was determined based on (a) **1a** and (b) **2a**.

To discuss the acid properties of Pt-M/ γ -Al₂O₃ (M = Mo, Re, W, and V) and Pt/ γ -Al₂O₃, we conducted pyridine FT-IR and NH₃-TPD measurements. The pyridine FT-IR spectrum of Pt-Mo/ γ -Al₂O₃ showed a strong peak at 1448 cm⁻¹ assigned to a Lewis acid site (Fig. S6a),^{S13} which is similar to that of Pt/ γ -Al₂O₃. The NH₃-TPD spectrum of Pt/ γ -Al₂O₃ exhibited two peaks at 161 and 292 °C, while all spectra of Pt-M/ γ -Al₂O₃ showed only one peak at 161 °C (Fig. S6b). Both pyridine FT-IR and NH₃-TPD spectra did not show any additional peaks by M loading. Thus, we could not identify the acid nature of MoO_x by pyridine FT-IR and NH₃-TPD.

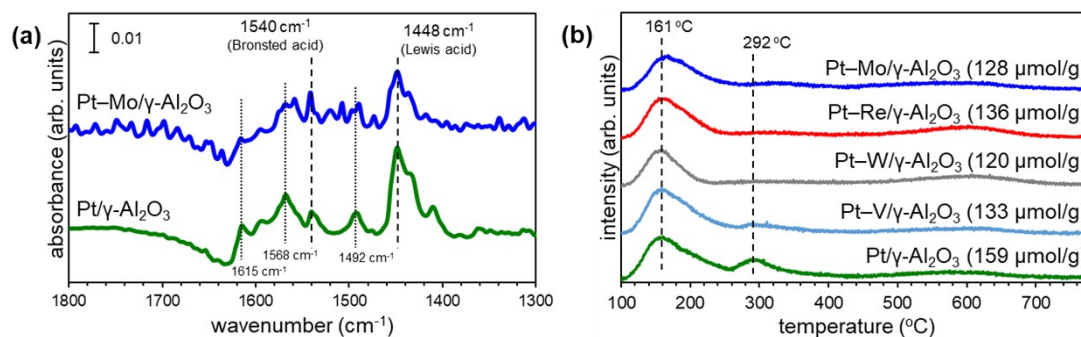


Fig. S6 (a) *In situ* pyridine adsorption FT-IR analysis of Pt-Mo/ γ -Al₂O₃, and Pt/ γ -Al₂O₃, and (b) NH₃-TPD profiles for Pt-M/ γ -Al₂O₃ (M = Mo, Re, W, or V) and Pt/ γ -Al₂O₃. Acid amount is presented in parentheses.

As shown in Fig. S7a, a slab model is constructed assuming the oxygen-vacant (011) surface of MoO₂ that consist of [Mo(IV)₄(H₂O)₄OH⁻₇O²⁻₆]³⁻ (model **A**). Cartesian coordinate of the MoO₂ surface is taken from a result of neutron powder diffraction.^{S14} In order to suppress a segmentation effect of the edge of the slab model, terminal oxygen ions (O²⁻) are capped by protons, and only the geometry of terminal protons is optimized. After that, to examine an adsorption of the **2a** on the surface, one **2a** is attached to the model **A** and only a structure of the **2a** molecule is optimized on the slab model as shown in Fig. S7b (model **B**). An isolated **2a** molecule is also optimized separately (model **C**).

The absorption energy (ΔE) is estimated by

$$\Delta E = \{E(\mathbf{A}) + E(\mathbf{C})\} - E(\mathbf{B}),$$

where $E(\mathbf{A})$, $E(\mathbf{B})$ and $E(\mathbf{C})$ are calculated total energies of the models **A**, **B** and **C**, respectively. $E(\mathbf{A})$, $E(\mathbf{B})$, $E(\mathbf{C})$ and ΔE are summarized in the table below.

Calculated total energies of models **A**, **B** and **C**. Adsorption energy is also summarized in the same table.

$E(\mathbf{B})$ / Hartree	$E(\mathbf{A})$ / Hartree	$E(\mathbf{C})$ / Hartree	ΔE / kcal mol ⁻¹
-1787.0328	-1557.8821	-229.07761	45.9

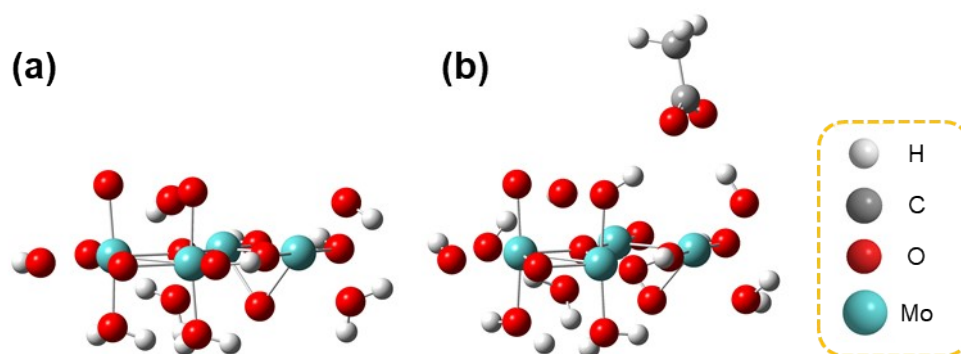


Fig. S7 Illustration of (a) model **A** and (b) model **B**.

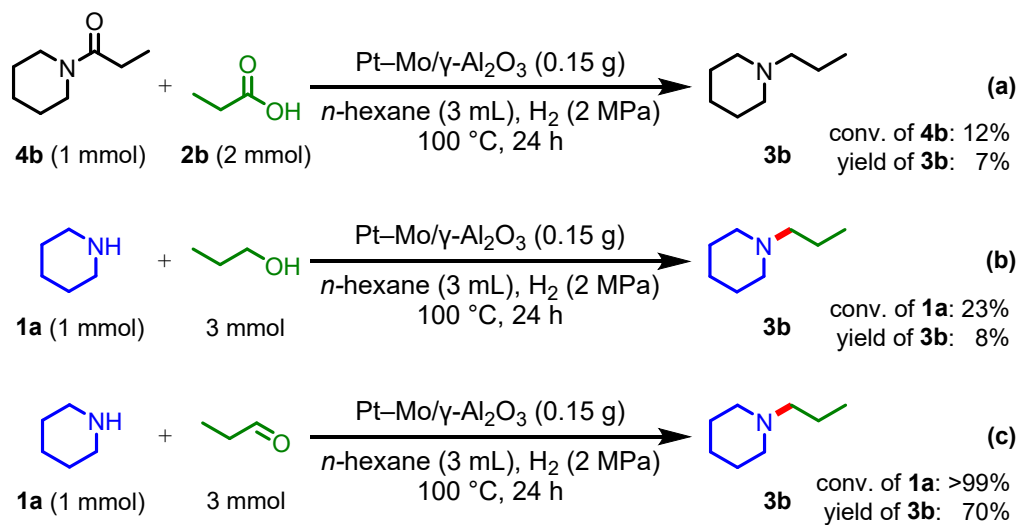
All calculations are performed under the gas phase condition by a spin unrestricted density functional theory (UDFT) with a use of Becke-3-parameter-Lee-Yang-Parr functional set. As basis set, 6-31G* (C, O, H) and Lanl2dz (Mo) are used. The spin state of the model is considered to be an open-shell singlet state. Cartesian coordinate of models **B** and **C** are summarized in the table below.

Cartesian coordinate of models **B** and **C**. (The model **A** is a substructure of model **B**).

Model B				Model C			
Atom	x / Å	y / Å	z / Å	Atom	x / Å	y / Å	z / Å
Mo	-0.07918	20.52424	-1.07663	C	-0.092462	0.125630	-0.000180
Mo	-3.43470	20.50702	-2.55746	O	-0.645667	1.201996	0.000034
Mo	-3.34533	20.70194	-5.06101	O	-0.778748	-1.046603	-0.000025
Mo	0.11567	20.61309	-3.58020	H	-1.723776	-0.802819	0.000368
O	-0.04661	19.04102	-2.39986	C	1.397605	-0.109871	-0.000034
O	-3.47156	22.48491	-2.39908	H	1.685643	-0.687150	0.884849
O	-4.91800	20.54806	-3.88034	H	1.685026	-0.696052	-0.879203
O	-1.86202	20.66090	-3.73813	H	1.917564	0.848319	-0.004808
O	-2.04858	20.57750	-1.01510				
O	-3.38775	22.67162	-5.12209				
O	1.89851	20.47644	-0.91871				
O	-4.79063	20.57134	-0.99439				
O	-1.98939	20.63762	-6.62408				
O	-4.73145	20.63146	-6.60337				
O	2.08506	20.55983	-3.64174				
O	-0.00071	21.90960	0.46602				
O	0.05847	21.96972	-5.14295				
H	0.02328	22.70807	-0.08816				
H	0.86694	21.82703	-5.66795				
H	2.27131	20.37701	-1.82275				
H	2.40687	20.20771	-4.49412				
H	-4.13323	20.84519	-0.33069				
H	-4.12136	20.99445	-7.27071				
H	-1.32216	21.30192	-6.31141				
O	-3.30847	18.72405	-5.21939				
O	-0.02199	19.16761	0.48612				
O	0.03720	19.22773	-5.12286				
O	-3.39228	18.53734	-2.49638				
H	0.94338	18.95546	0.54221				
H	-0.44340	18.46275	-4.73676				
H	-2.83179	17.99941	-3.19538				

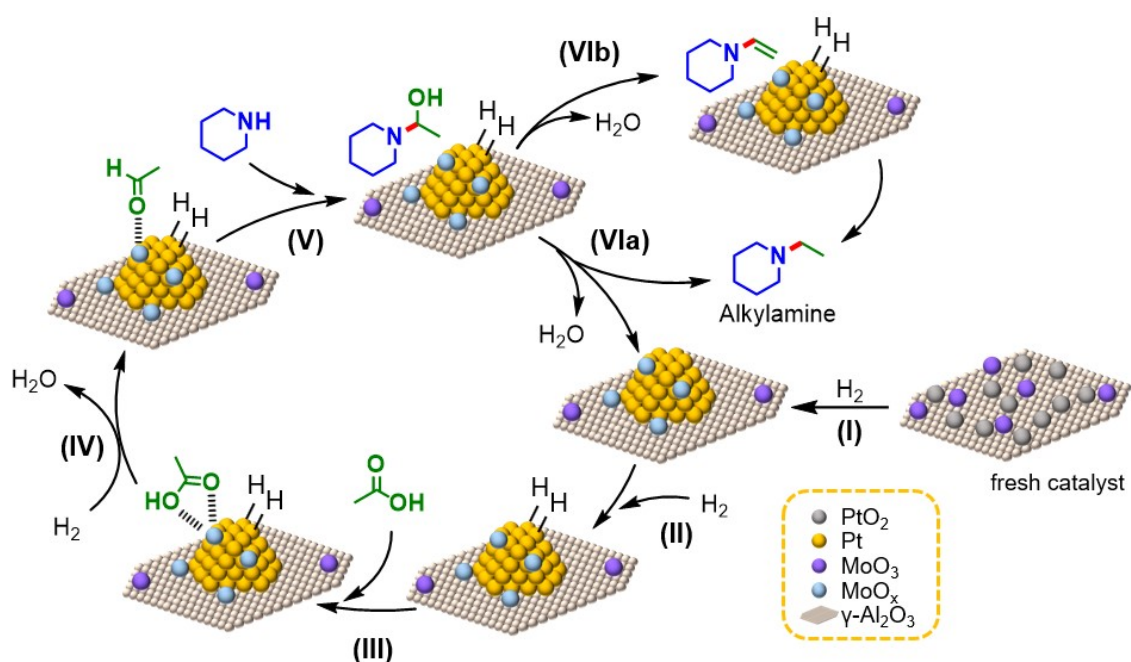
H	-2.96476	18.64399	-6.13492
H	-0.16988	19.74839	1.27328
H	-0.58897	19.62730	-5.80574
H	-2.63488	18.04522	-4.65449
H	-2.84478	18.44101	-1.68056
C	-1.07128	24.96832	-0.85743
O	0.05591	24.40569	-0.79838
O	-2.22116	24.47868	-0.74625
H	-2.91559	22.96489	-1.73656
C	-1.03413	26.50742	-1.14036
H	-1.23297	26.67400	-2.20784
H	-1.82283	27.02473	-0.57744
H	-0.05491	26.94176	-0.89957

5. Supplementary schemes



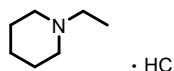
Scheme S1 Control experiments. (a) Hydrogenation of **4b**. (b) Amination of 1-propanol with **1a**. (c) Reductive amination of propionaldehyde with **1a**.

A major reaction pathway is proposed as shown in Scheme S2. First, Pt NPs are formed via reduction with H_2 and dissociate H_2 to reduce MoO_3 to MoO_x (step I). Then, hydrogen species are formed on the Pt NPs (step II). Carboxylic acid is adsorbed on the MoO_x (step III). Activated carboxylic acid is hydrogenated to aldehyde (step IV) followed by the attack of amine to the activated aldehyde to form hemiaminal intermediate (step V). Finally, hydrogenation of hemiaminal affords alkylamine (step VI). The steps VIa and VIb in Scheme S2 was supported by the following experimental results: the amination of acetic acid- d_4 (**21**) afforded *N*-ethyl piperidine with H–D scrambling (Scheme 3a). Thus, there are two reaction pathways to afford amine, i.e., via a direct hydrogenation of hemiaminal (step VIa) or through enamine (step VIb).



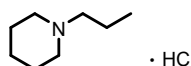
Scheme S2 Proposed major reaction path for the reductive amination of **2a** with **1a** over a Pt–Mo/ γ - Al_2O_3 .

6. Product identification



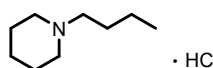
***N*-ethyl piperidine hydrochloride**

CAS registry No. [17874-60-1]. **¹H NMR** (400 MHz, D₂O): δ/ppm 3.52 (d, 2H, *J* = 12.4 Hz), 3.14 (dq, 2H, *J* = 7.2, 2.4 Hz), 2.90 (t, 2H, *J* = 12.4 Hz), 1.95 (d, 2H, *J* = 14.0 Hz), 1.86–1.78 (m, 1H), 1.78–1.63 (m, 2H), 1.54–1.41 (m, 1H), 1.30 (dt, 3H, *J* = 7.4 Hz, 3.2 Hz). **¹³C NMR** (100 MHz, D₂O): δ/ppm 53.1, 52.7, 23.5, 21.8, 9.2. **GC-MS** (EI): 113.10.



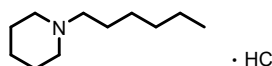
***N*-propyl piperidine hydrochloride**

CAS registry No. [17874-62-3]. **¹H NMR** (400 MHz, D₂O): δ/ppm 3.52 (d, 2H, *J* = 12.4 Hz), 3.12–2.96 (m, 2H), 2.91 (dt, 2H, *J* = 12.4, 1.6 Hz), 1.94 (d, 2H, *J* = 14.4 Hz), 1.87–1.64 (m, 5H), 1.55–1.41 (m, 1H), 0.96 (t, 3H, *J* = 7.4 Hz). **¹³C NMR** (100 MHz, D₂O): δ/ppm 59.0, 53.6, 23.4, 21.8, 17.7, 10.8. **GC-MS** (EI): 127.15.



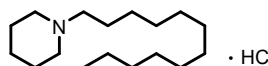
***N*-butyl piperidine hydrochloride**

CAS registry No. [80840-88-6]. **¹H NMR** (400 MHz, D₂O): δ/ppm 3.53 (d, 2H, *J* = 12.8 Hz), 3.12–3.04 (m, 2H), 2.91 (dt, 2H, *J* = 12.8, 2.0 Hz), 1.94 (d, 2H, *J* = 14.4 Hz), 1.86–1.64 (m, 5H), 1.54–1.30 (m, 3H), 0.93 (t, 3H, *J* = 7.4 Hz). **¹³C NMR** (100 MHz, D₂O): δ/ppm 57.3, 53.6, 26.0, 23.4, 21.8, 19.9, 13.4. **GC-MS** (EI): 141.15.



***N*-hexyl piperidine hydrochloride**

CAS registry No. [80840-90-0]. **¹H NMR** (400 MHz, D₂O): δ/ppm 3.52 (d, 2H, *J* = 12.4 Hz), 3.13–3.03 (m, 2H), 2.91 (dt, 2H, *J* = 12.6, 2.0 Hz), 1.94 (d, 2H, *J* = 14.4 Hz), 1.86–1.65 (m, 5H), 1.53–1.41 (m, 1H), 1.40–1.25 (m, 6H), 0.88 (t, 3H, *J* = 7.2 Hz). **¹³C NMR** (100 MHz, D₂O): δ/ppm 57.6, 53.6, 31.0, 26.0, 23.9, 23.4, 22.3, 21.8, 13.9. **GC-MS** (EI): 169.20.



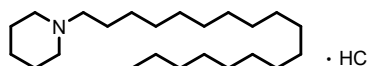
***N*-dodecyl piperidine hydrochloride**

CAS registry No. [71756-81-5]. **¹H NMR** (400 MHz, CDCl₃): δ/ppm 11.9 (br-s, 1H), 3.52 (d, 2H, *J* = 11.2 Hz), 2.99–2.87 (m, 2H), 2.76–2.60 (m, 2H), 2.38–2.20 (m, 2H), 2.00–1.79 (m, 5H), 1.52–1.18 (m, 19H), 0.88 (t, 3H, *J* = 6.8 Hz). **¹³C NMR** (100 MHz, CDCl₃): δ/ppm 57.4, 53.0, 31.8, 29.50, 29.48, 29.40, 29.3, 29.2, 29.0, 26.8, 23.4, 22.6, 22.5, 22.1, 14.0. **GC-MS** (EI): 253.25.



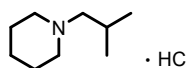
N-hexadecyl piperidine hydrochloride

CAS registry No. [89632-30-4]. ¹H NMR (400 MHz, CDCl₃): δ/ppm 11.8 (br-s, 1H), 3.53 (d, 2H, *J* = 10.8 Hz), 3.02–2.83 (m, 2H), 2.75–2.58 (m, 2H), 2.40–2.13 (m, 2H), 2.00–1.78 (m, 4H), 1.50–1.05 (m, 28H), 0.88 (t, 3H, *J* = 7.0 Hz). ¹³C NMR (100 MHz, CDCl₃): δ/ppm 57.5, 53.0, 31.8, 29.63, 29.60, 29.57, 29.50, 29.4, 29.33, 29.28, 29.0, 26.8, 23.4, 22.6, 22.5, 22.1, 14.1. GC-MS (EI): 309.30.



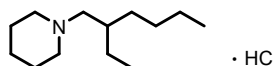
N-octadecyl piperidine hydrochloride

CAS registry No. [89632-31-5]. ¹H NMR (400 MHz, CDCl₃): δ/ppm 11.9 (br-s, 1H), 3.51 (d, 2H, *J* = 10.4 Hz), 3.00–2.85 (m, 2H), 2.75–2.59 (m, 2H), 2.40–2.23 (m, 2H), 2.00–1.78 (m, 4H), 1.55–1.00 (m, 32H), 0.88 (t, 3H, *J* = 7.0 Hz). ¹³C NMR (100 MHz, CDCl₃): δ/ppm 57.5, 53.0, 31.9, 29.63, 29.59, 29.5, 29.4, 29.33, 29.29, 29.0, 26.9, 23.4, 22.6, 22.5, 22.1, 14.1. GC-MS (EI): 337.40.



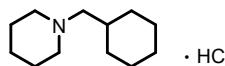
N-isobutyl piperidine hydrochloride

CAS registry No. [858850-36-9]. ¹H NMR (400 MHz, D₂O): δ/ppm 3.53 (d, 2H, *J* = 12.0 Hz), 3.00–2.87 (m, 4H), 2.21–2.09 (m, 1H), 1.99–1.88 (m, 2H), 1.86–1.69 (m, 3H), 1.56–1.42 (m, 1H), 0.99 (d, 6H, *J* = 7.2 Hz). ¹³C NMR (100 MHz, D₂O): δ/ppm 64.5, 54.0, 23.7, 23.0, 21.7, 19.9. GC-MS (EI): 141.15.



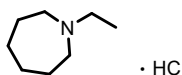
N-(2-ethylhexyl) piperidine hydrochloride

CAS registry No. [1071548-49-6]. ¹H NMR (400 MHz, D₂O): δ/ppm 3.57–3.47 (m, 2H), 3.02 (d, 2H, *J* = 7.2 Hz), 2.99–2.86 (m, 2H), 1.93 (d, 2H, *J* = 14.4 Hz), 1.88–1.67 (m, 4H), 1.58–1.22 (m, 9H), 0.99–0.80 (m, 6H). ¹³C NMR (100 MHz, D₂O): δ/ppm 61.5, 54.4, 54.0, 34.2, 30.3, 28.1, 23.8, 22.9, 22.8, 21.7, 13.9, 9.9. GC-MS (EI): 197.20.



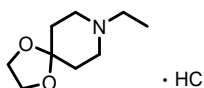
N-cyclohexylmethyl piperidine hydrochloride

CAS registry No. [5005-71-0]. ¹H NMR (400 MHz, D₂O): δ/ppm 3.52 (d, 2H, *J* = 12.4 Hz), 3.02–2.82 (m, 4H), 2.01–1.60 (m, 11H), 1.56–1.41 (m, 1H), 1.38–1.11 (m, 3H), 1.09–0.94 (m, 2H). ¹³C NMR (100 MHz, D₂O): δ/ppm 63.4, 54.0, 32.7, 30.6, 26.0, 25.5, 23.0, 21.7. GC-MS (EI): 181.20.



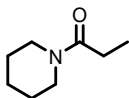
***N*-ethyl hexamethyleneimine hydrochloride**

CAS registry No. [6763-92-4]. **¹H NMR** (400 MHz, D₂O): δ/ppm 3.50–3.39 (m, 2H), 3.28–3.12 (m, 4H), 2.00–1.89 (m, 2H), 1.89–1.76 (m, 2H), 1.76–1.62 (m, 4H), 1.31 (t, 3H, *J* = 7.2 Hz). **¹³C NMR** (100 MHz, D₂O): δ/ppm 54.7, 53.2, 26.3, 24.1, 9.6. **GC-MS** (EI): 127.20.



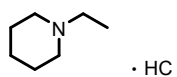
***N*-ethyl 4-piperidone ethylene ketal hydrochloride**

¹H NMR (400 MHz, D₂O): δ/ppm 4.08 (s, 4H), 3.67–3.60 (m, 2H), 3.28–3.09 (m, 4H), 2.14–1.98 (m, 4H), 1.33 (t, 3H, *J* = 7.4 Hz). **¹³C NMR** (100 MHz, D₂O): δ/ppm 104.8, 65.2, 65.1, 52.2, 50.7, 32.1, 9.5. **GC-MS** (EI): 171.15.

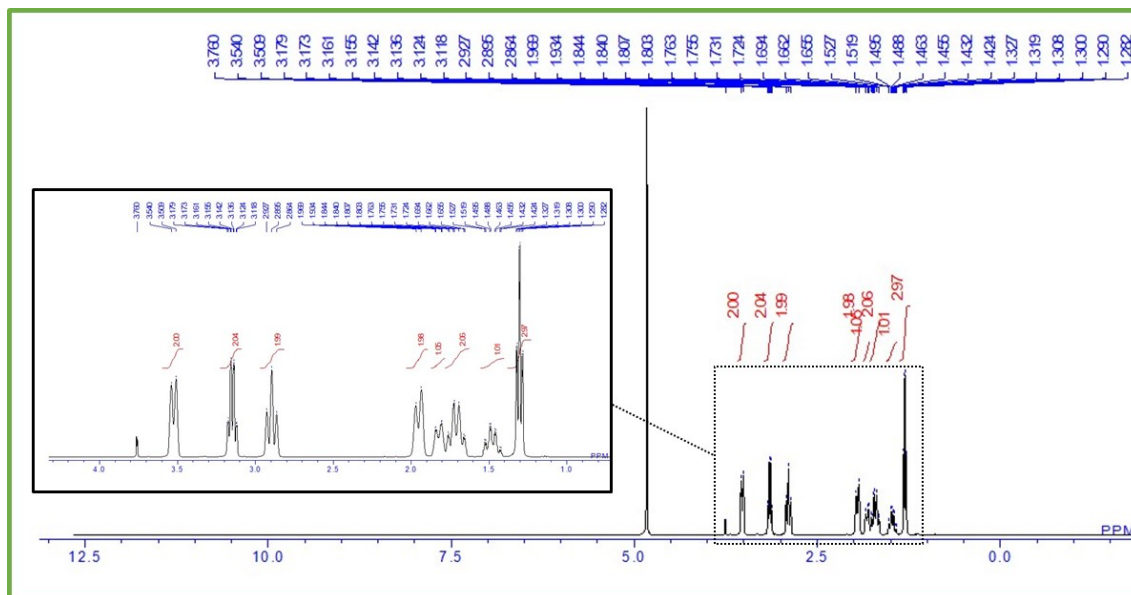


***N*-propionylpiperidine**

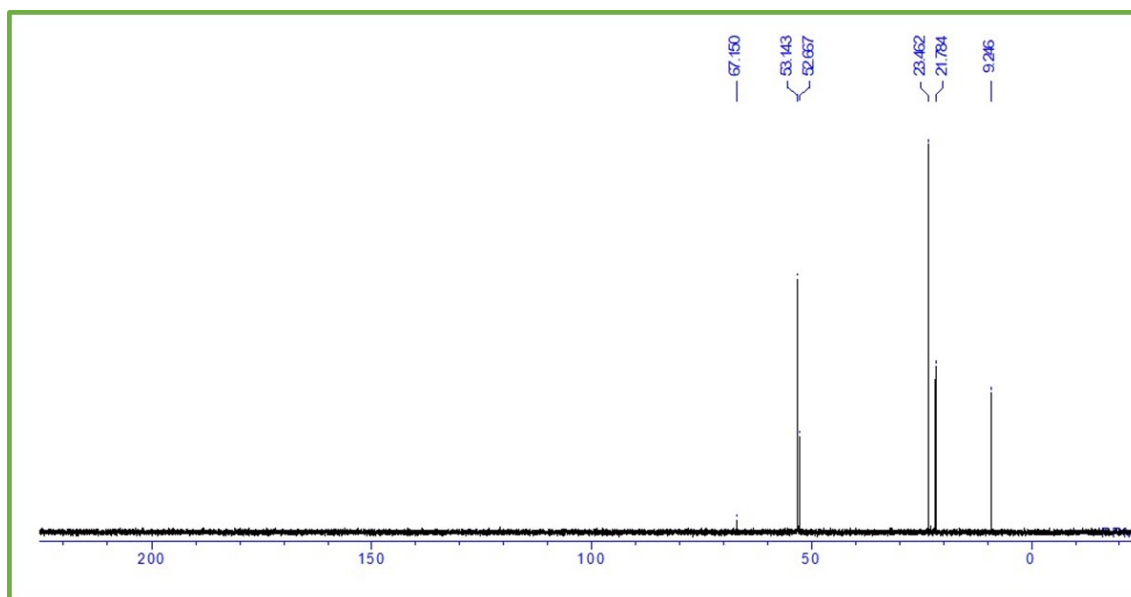
CAS registry No. [14045-28-4]. **¹H NMR** (400 MHz, CDCl₃): δ/ppm 3.55 (t, 2H, *J* = 5.6 Hz), 3.40 (t, 2H, *J* = 5.6 Hz), 2.34 (q, 2H, *J* = 7.6 Hz), 1.68–1.60 (m, 2H), 1.60–1.49 (m, 4H), 1.14 (t, 3H, *J* = 7.6 Hz). **¹³C NMR** (100 MHz, CDCl₃): δ/ppm 172.0, 46.4, 42.5, 26.5, 26.4, 25.5, 24.5, 9.5. **GC-MS** (EI): 141.15.



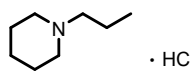
N-ethyl piperidine hydrochloride



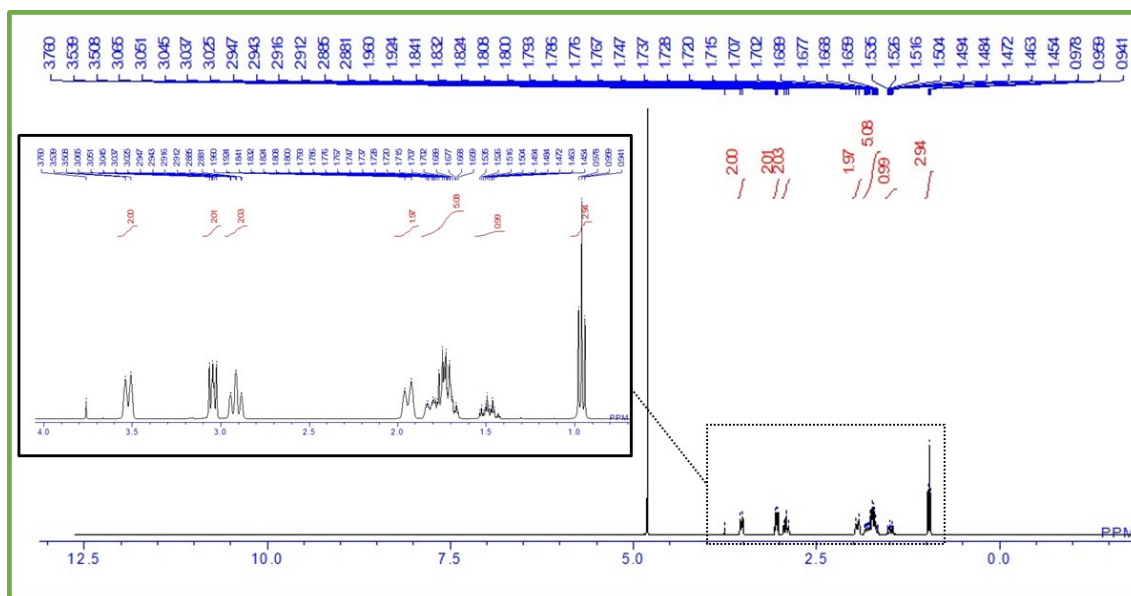
¹H NMR spectrum of *N*-ethyl piperidine hydrochloride



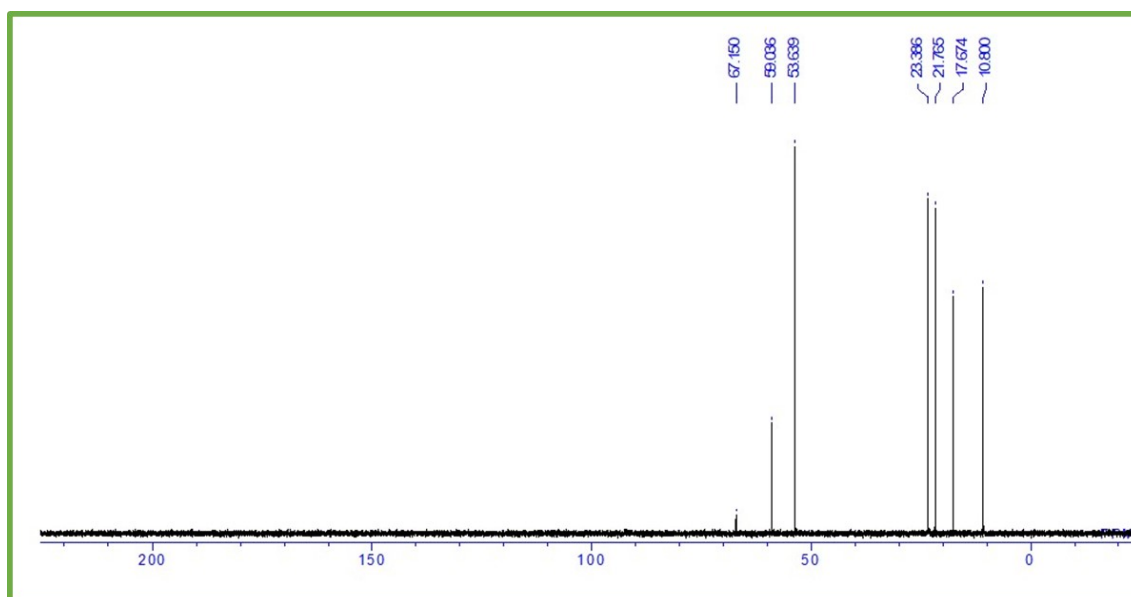
¹³C NMR spectrum of *N*-ethyl piperidine hydrochloride



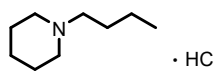
***N*-propyl piperidine hydrochloride**



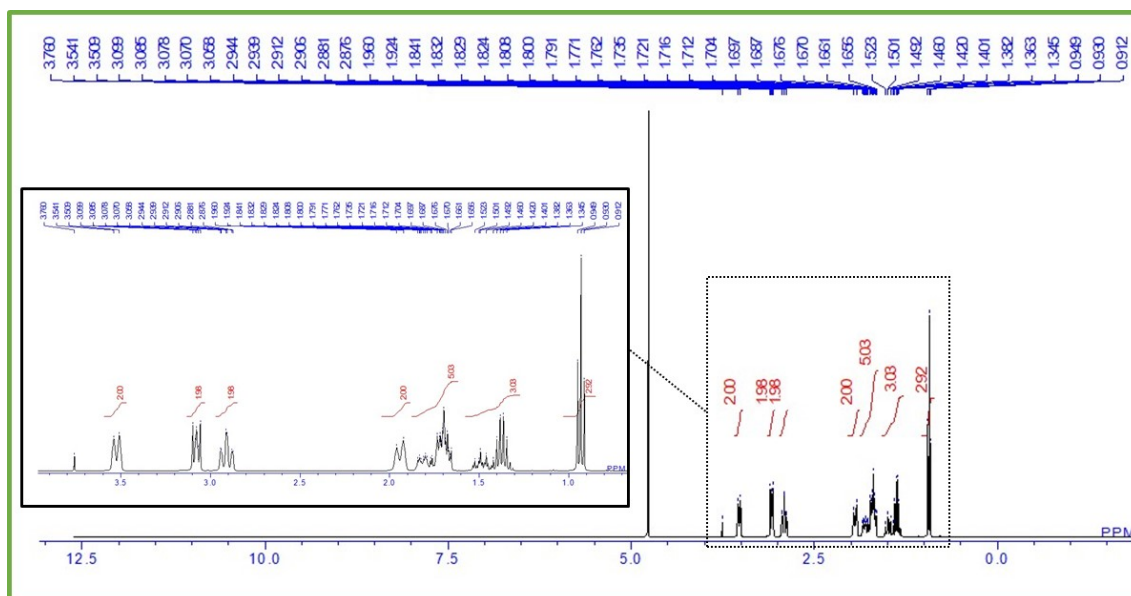
¹H NMR spectrum of *N*-propyl piperidine hydrochloride



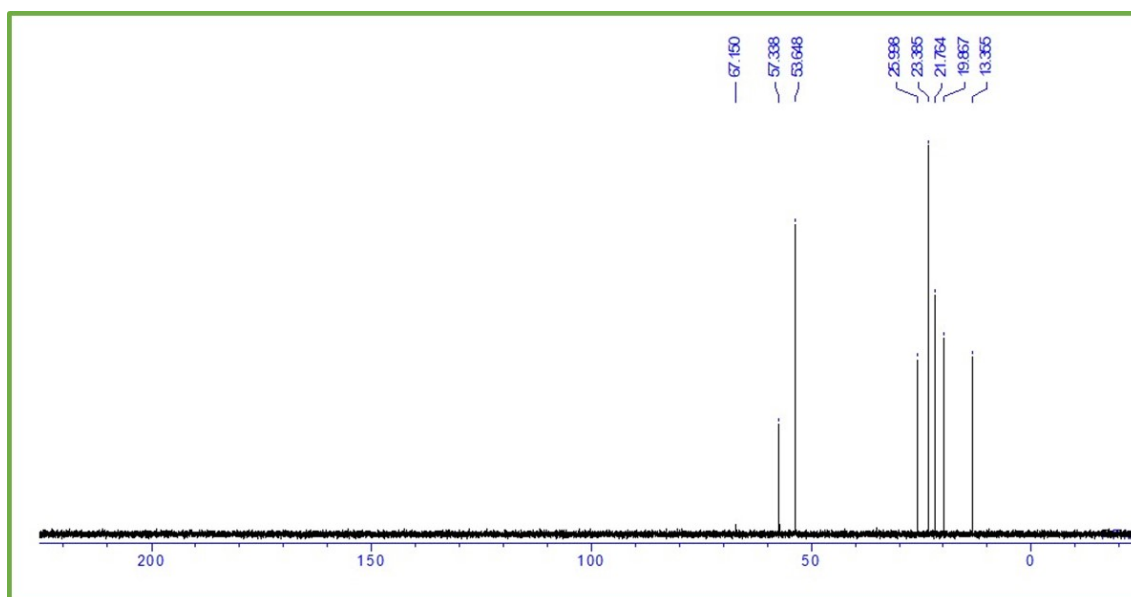
¹³C NMR spectrum of *N*-propyl piperidine hydrochloride



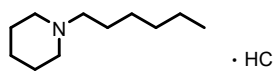
***N*-butyl piperidine hydrochloride**



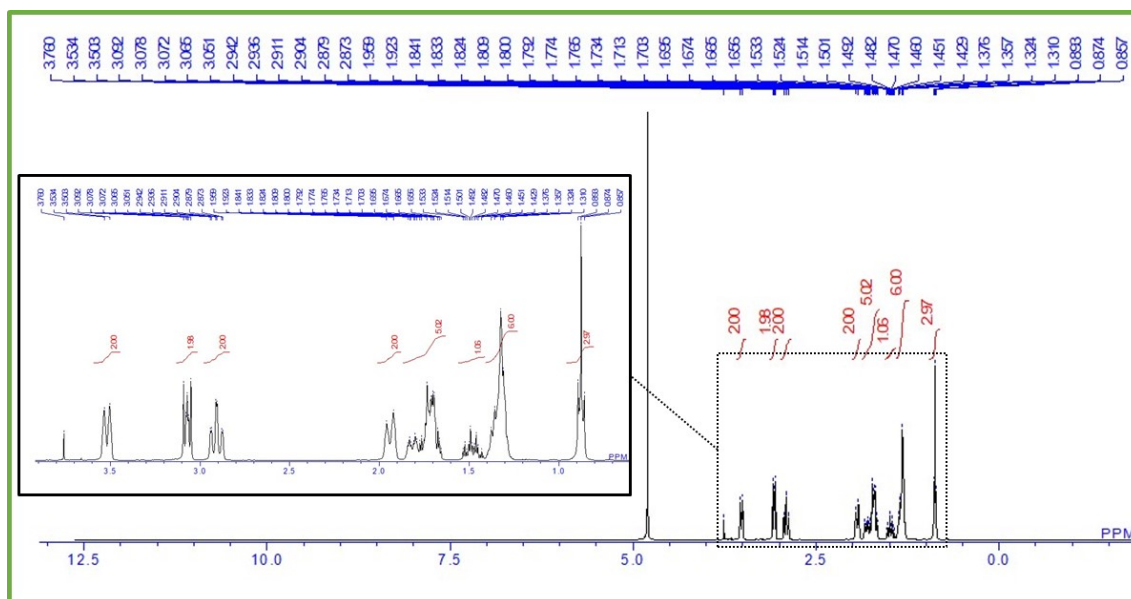
¹H NMR spectrum of *N*-butyl piperidine hydrochloride



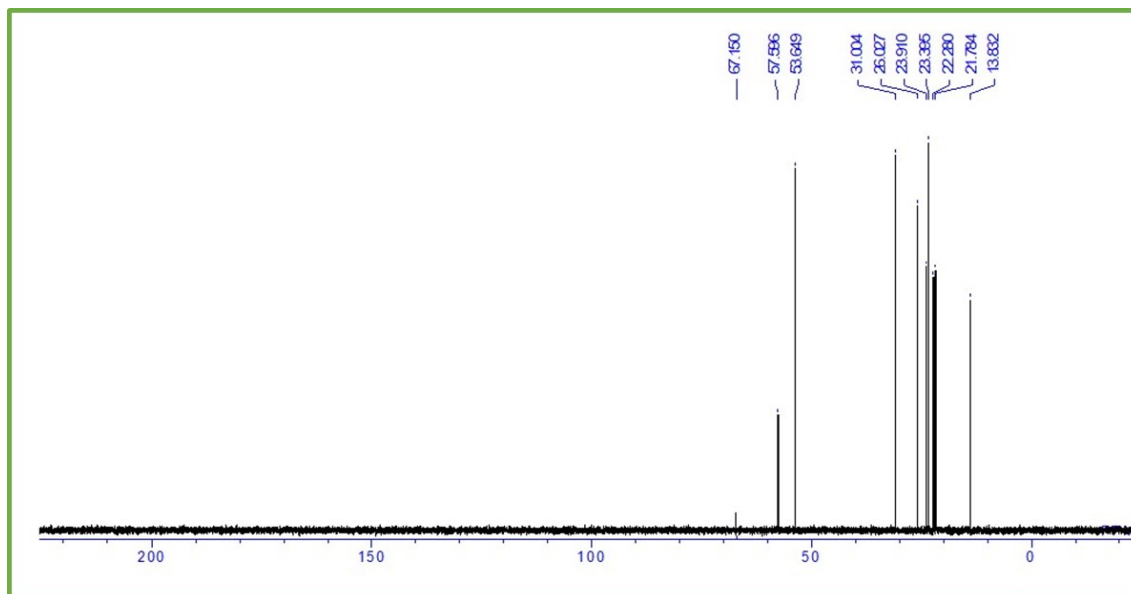
¹³C NMR spectrum of *N*-butyl piperidine hydrochloride



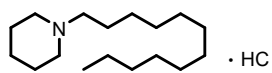
***N*-hexyl piperidine hydrochloride**



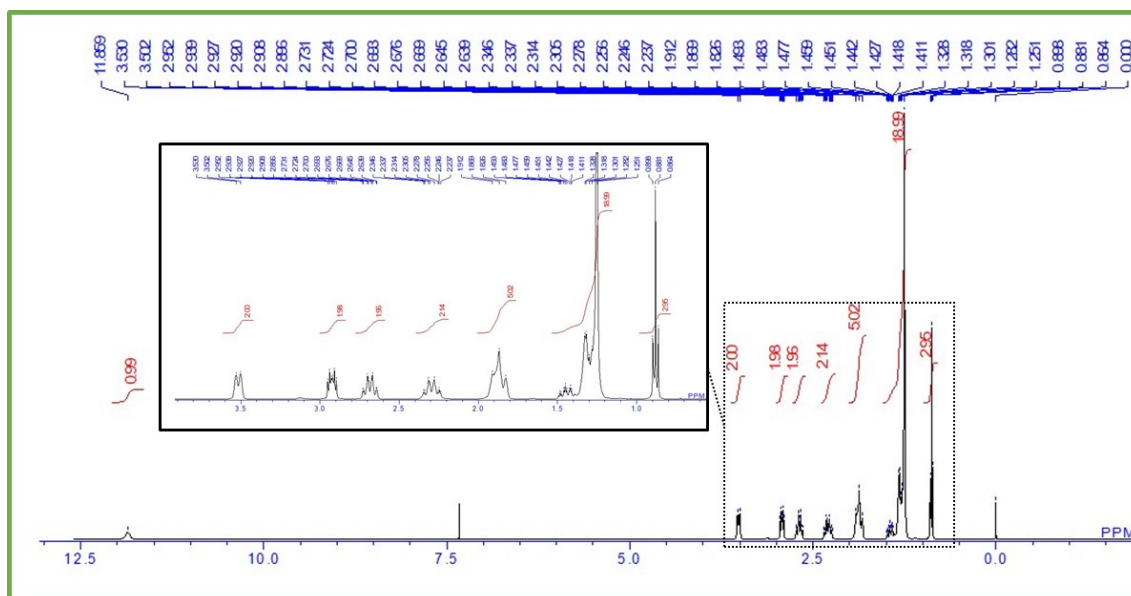
¹H NMR spectrum of *N*-hexyl piperidine hydrochloride



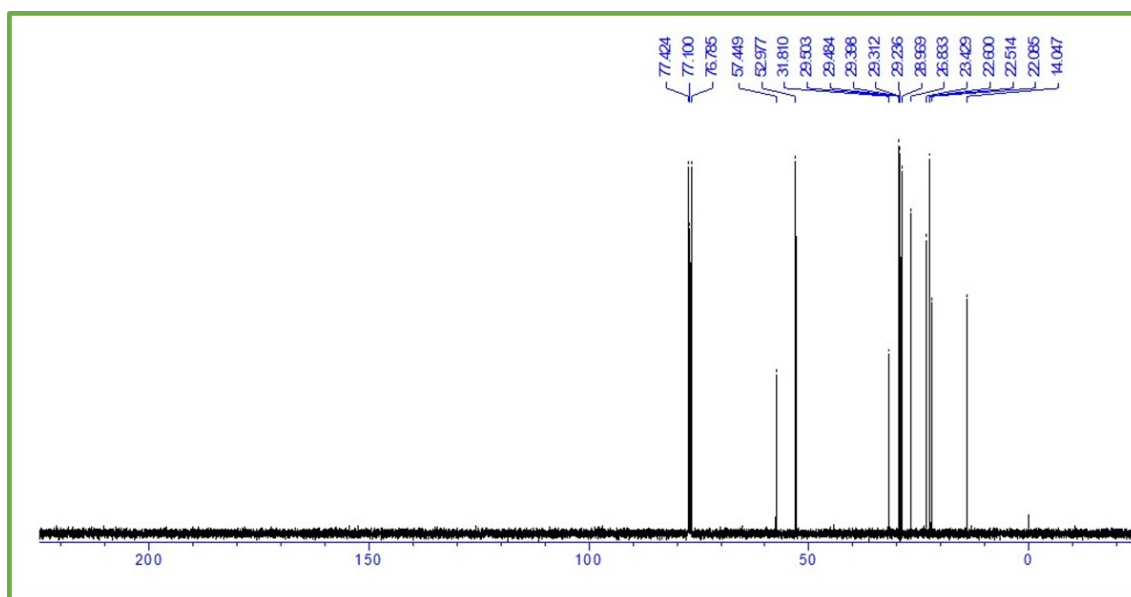
¹³C NMR spectrum of *N*-hexyl piperidine hydrochloride



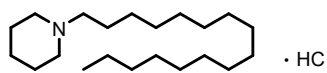
***N*-dodecyl piperidine hydrochloride**



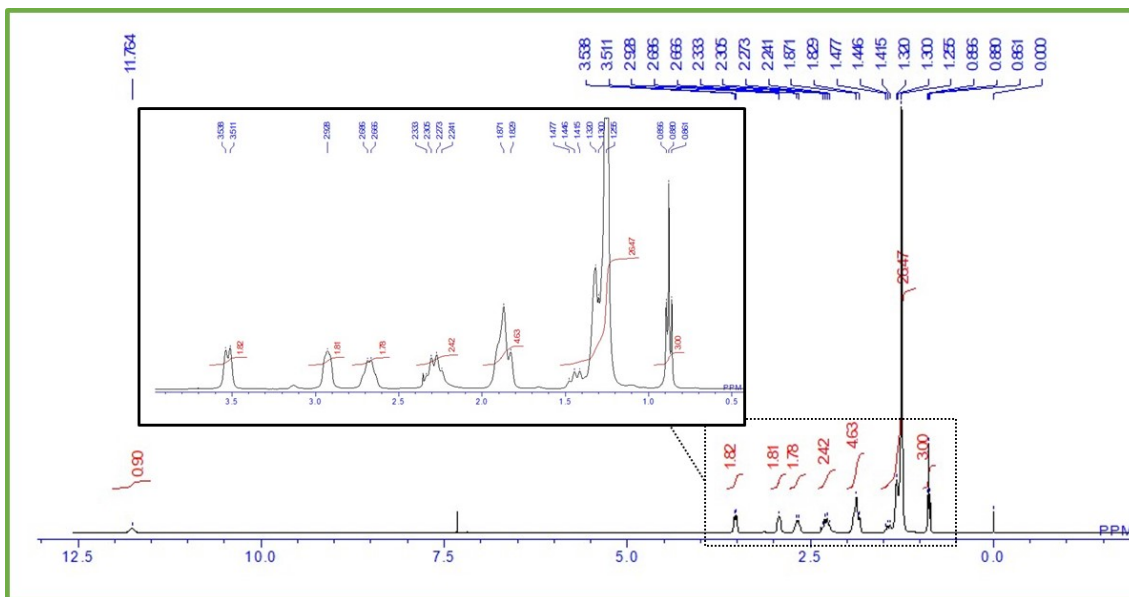
¹H NMR spectrum of *N*-dodecyl piperidine hydrochloride



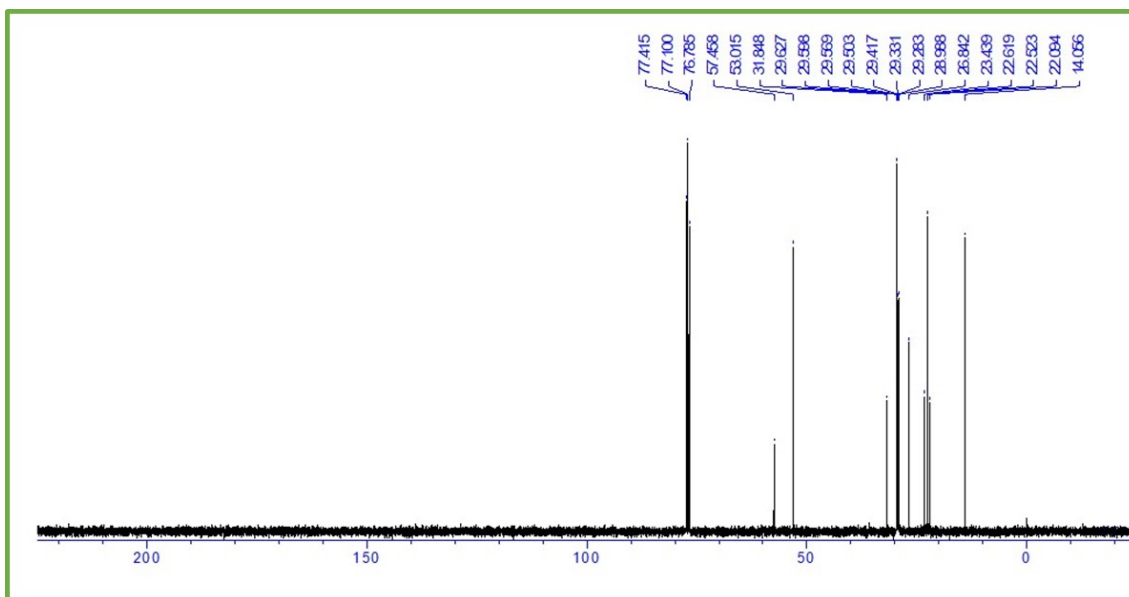
¹³C NMR spectrum of *N*-dodecyl piperidine hydrochloride



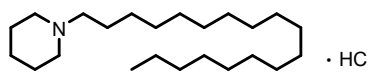
***N*-hexadecyl piperidine hydrochloride**



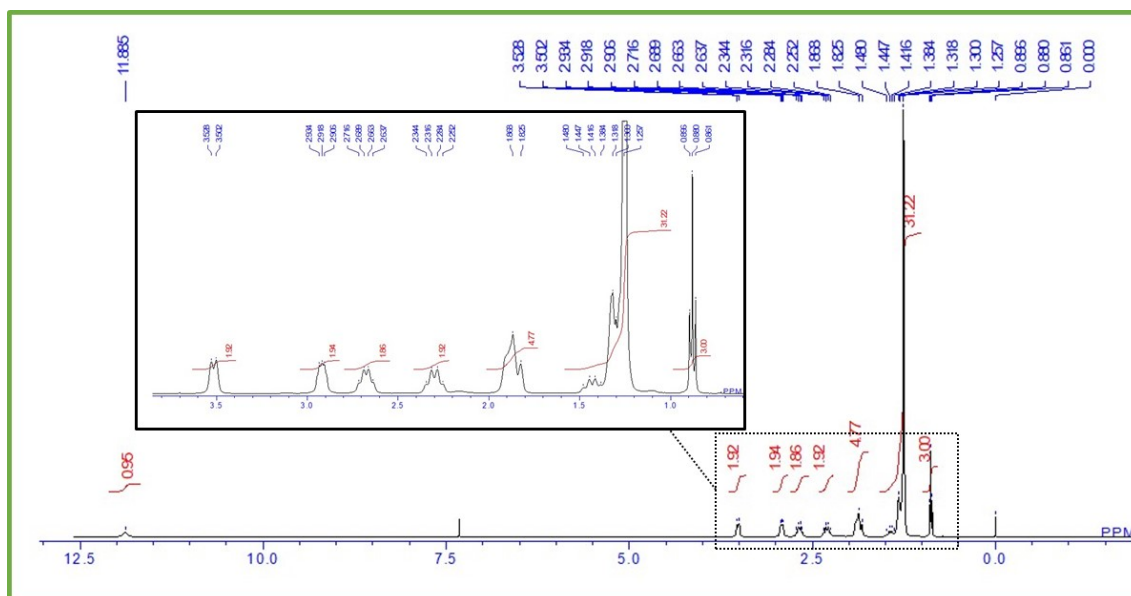
¹H NMR spectrum of *N*-hexadecyl piperidine hydrochloride



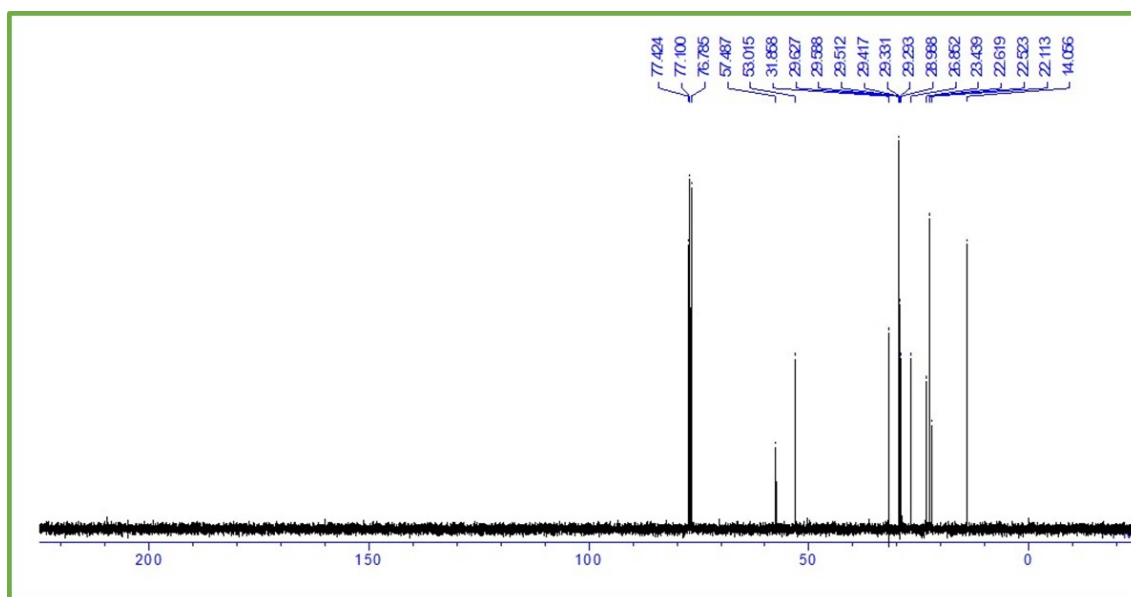
¹³C NMR spectrum of *N*-hexadecyl piperidine hydrochloride



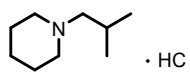
N-octadecyl piperidine hydrochloride



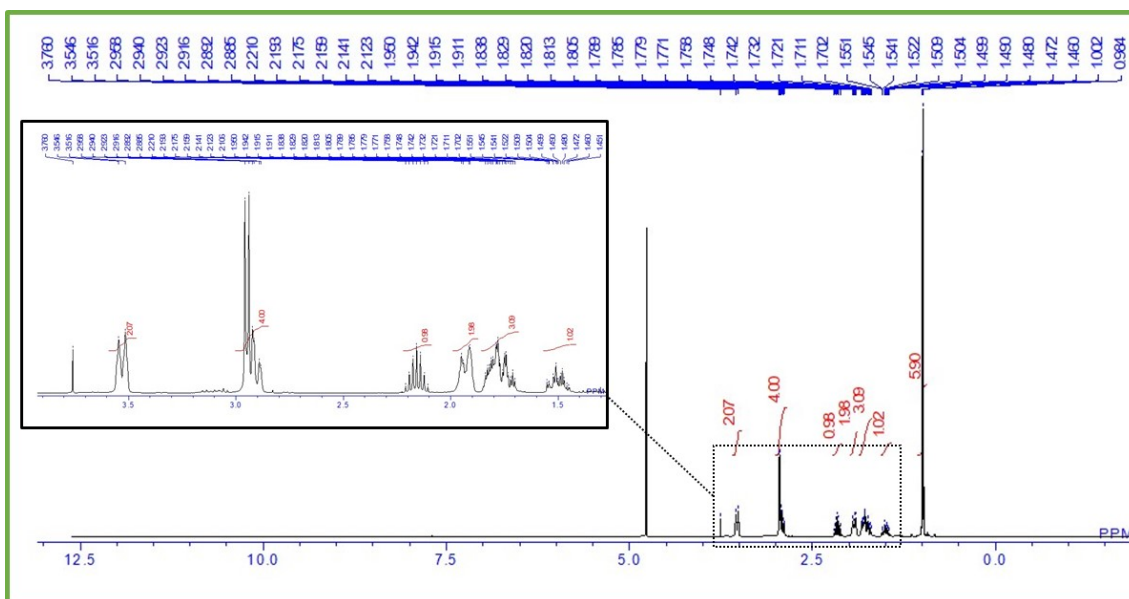
^1H NMR spectrum of *N*-octadecyl piperidine hydrochloride



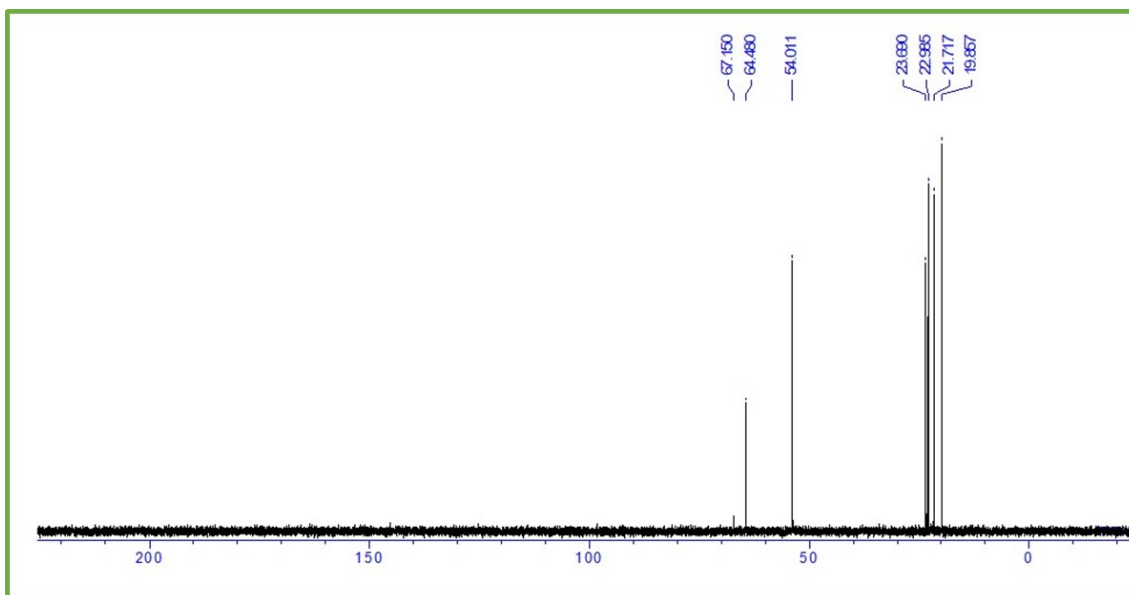
^{13}C NMR spectrum of *N*-octadecyl piperidine hydrochloride



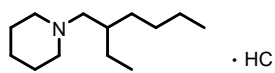
N-isobutyl piperidine hydrochloride



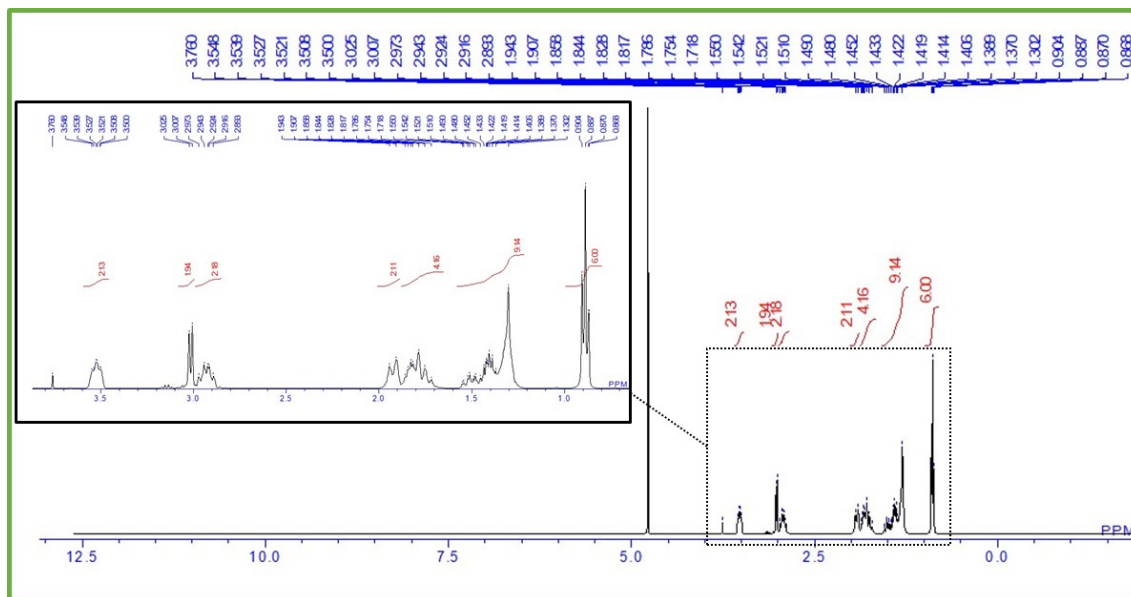
¹H NMR spectrum of *N*-isobutyl piperidine hydrochloride



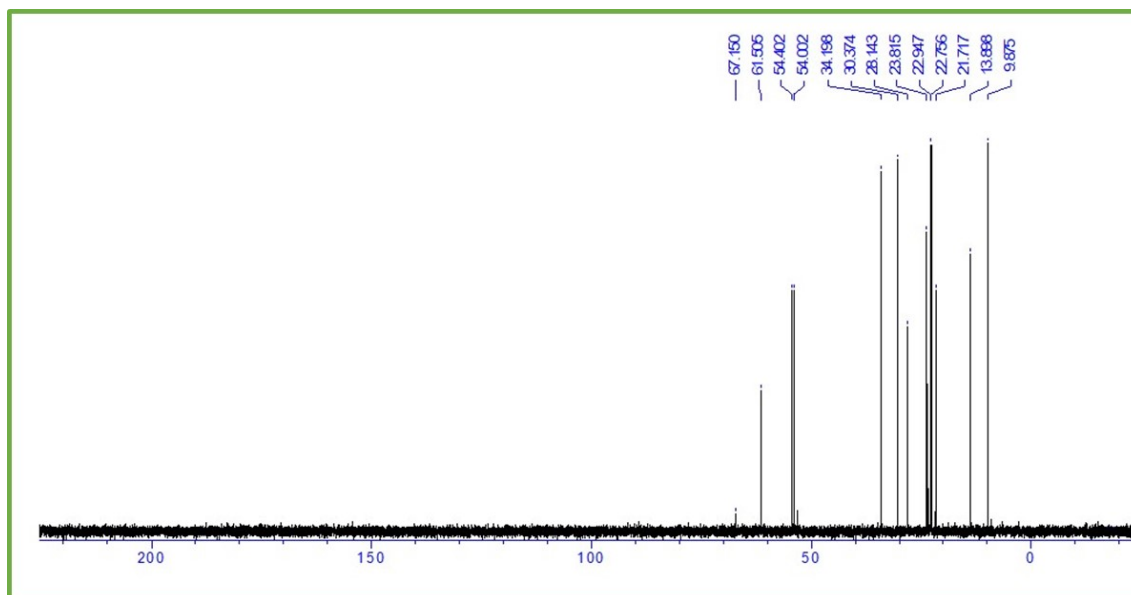
¹³C NMR spectrum of *N*-isobutyl piperidine hydrochloride



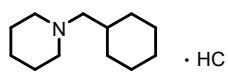
***N*-(2-ethylhexyl) piperidine hydrochloride**



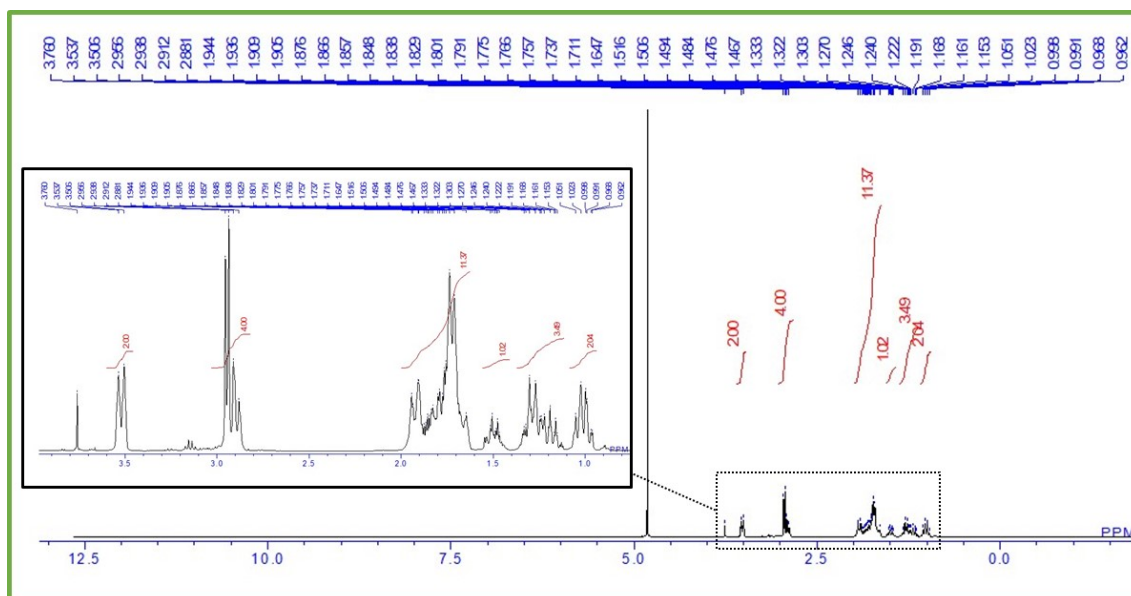
¹H NMR spectrum of *N*-(2-ethylhexyl) piperidine hydrochloride



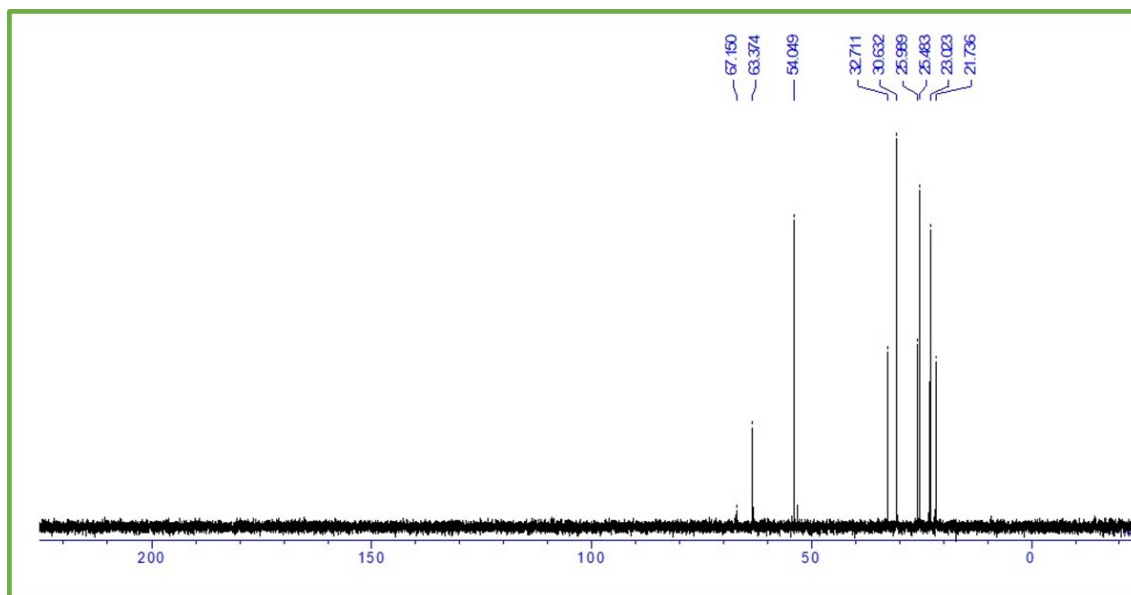
¹³C NMR spectrum of *N*-(2-ethylhexyl) piperidine hydrochloride



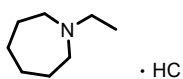
***N*-cyclohexylmethyl piperidine hydrochloride**



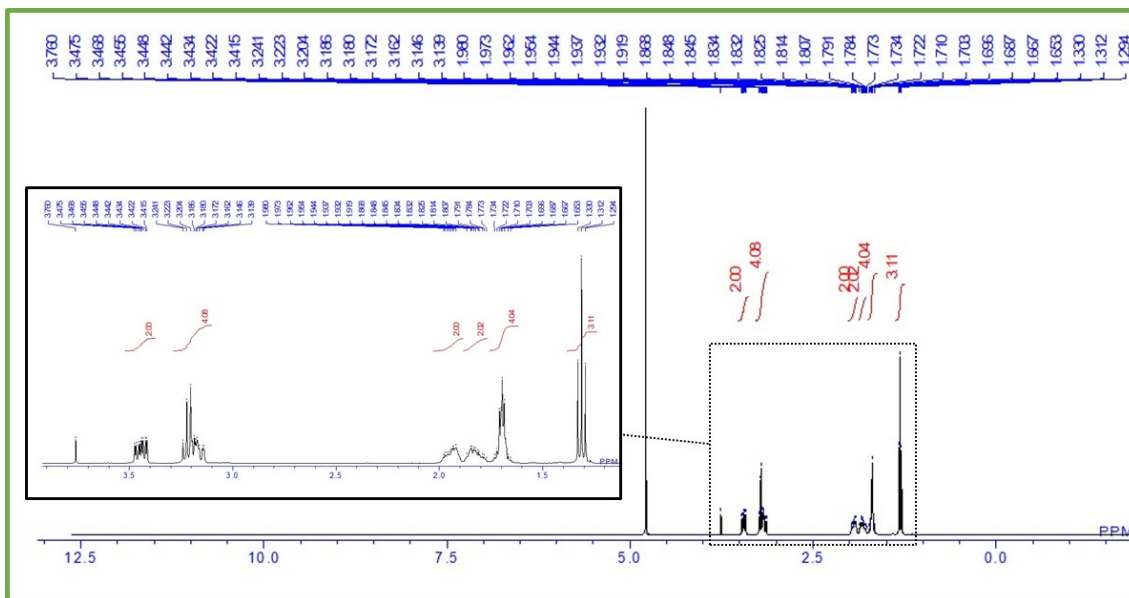
¹H NMR spectrum of *N*-cyclohexylmethyl piperidine hydrochloride



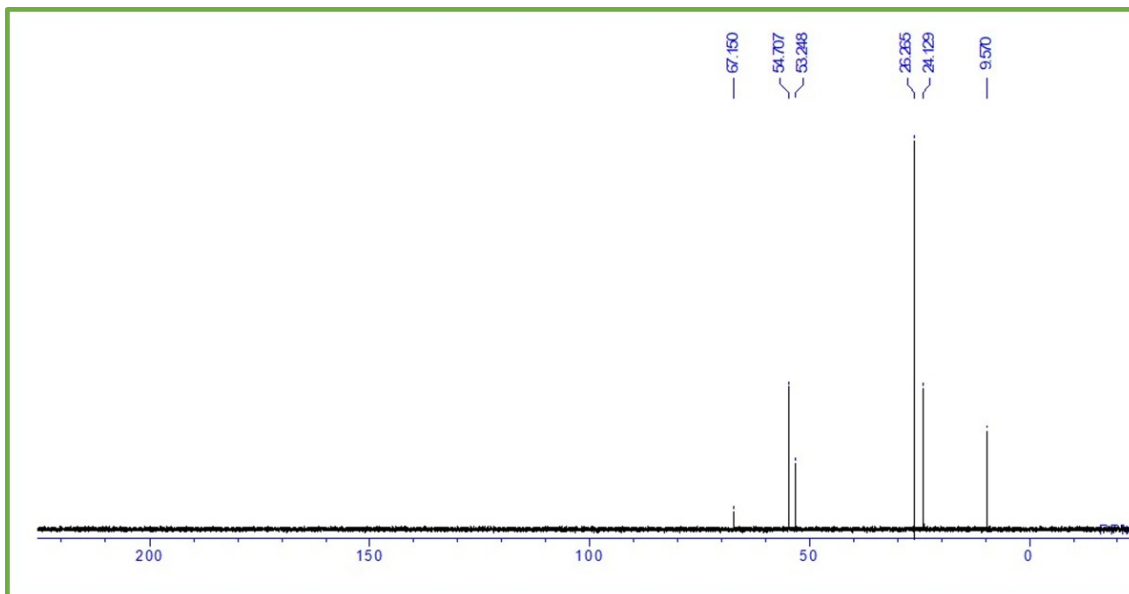
¹³C NMR spectrum of *N*-cyclohexylmethyl piperidine hydrochloride



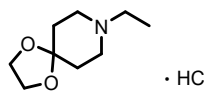
***N*-ethyl hexamethyleneimine hydrochloride**



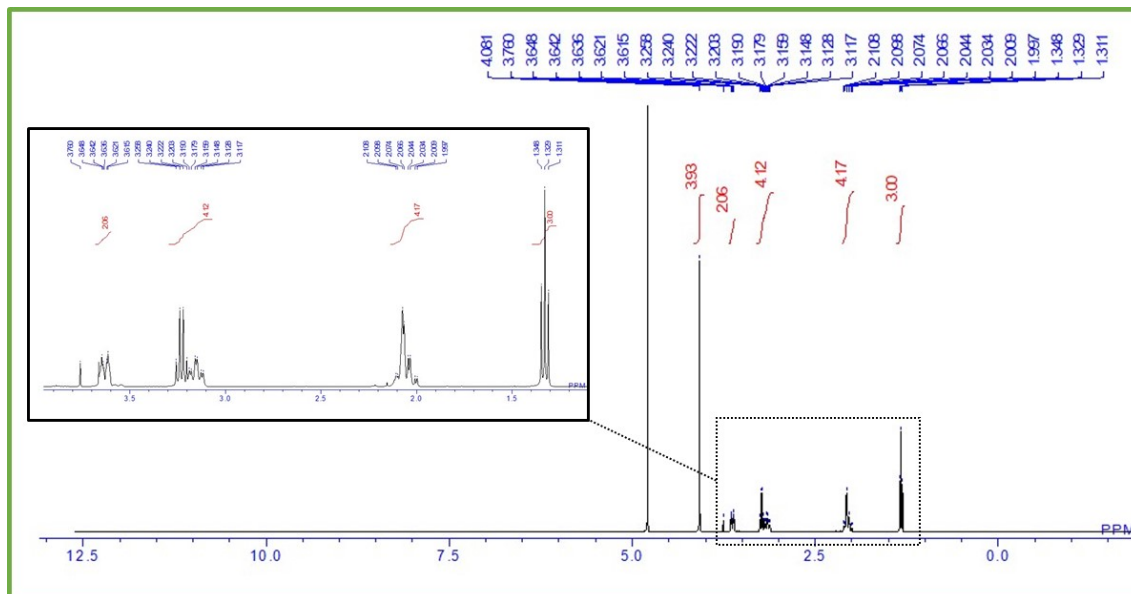
¹H NMR spectrum of *N*-ethyl hexamethyleneimine hydrochloride



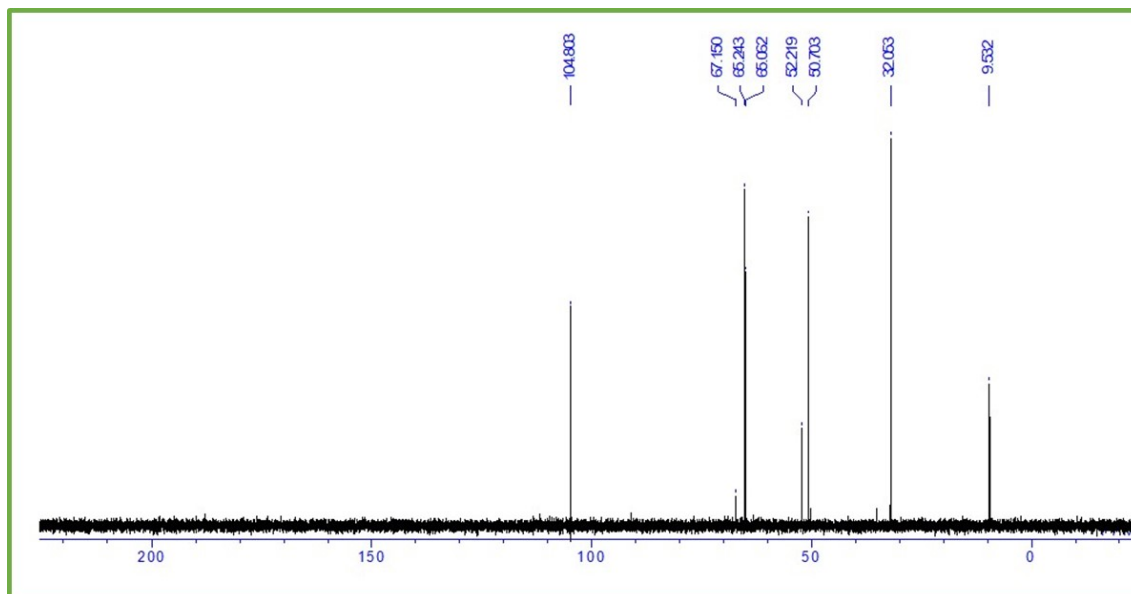
¹³C NMR spectrum of *N*-ethyl hexamethyleneimine hydrochloride



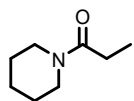
***N*-ethyl 4-piperidone ethylene ketal hydrochloride**



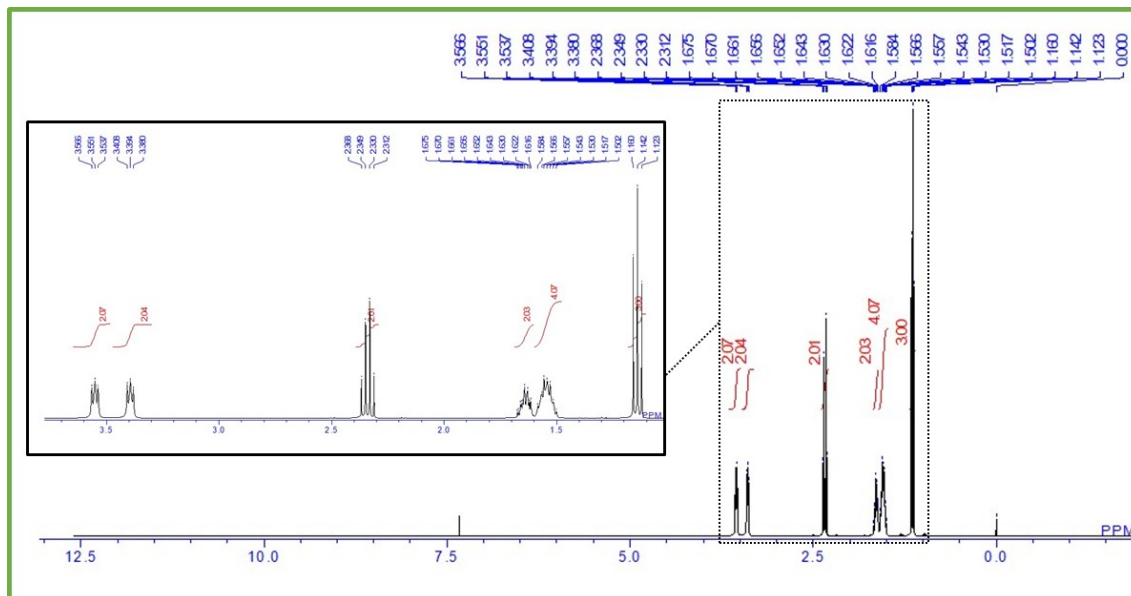
¹H NMR spectrum of *N*-ethyl 4-piperidone ethylene ketal hydrochloride



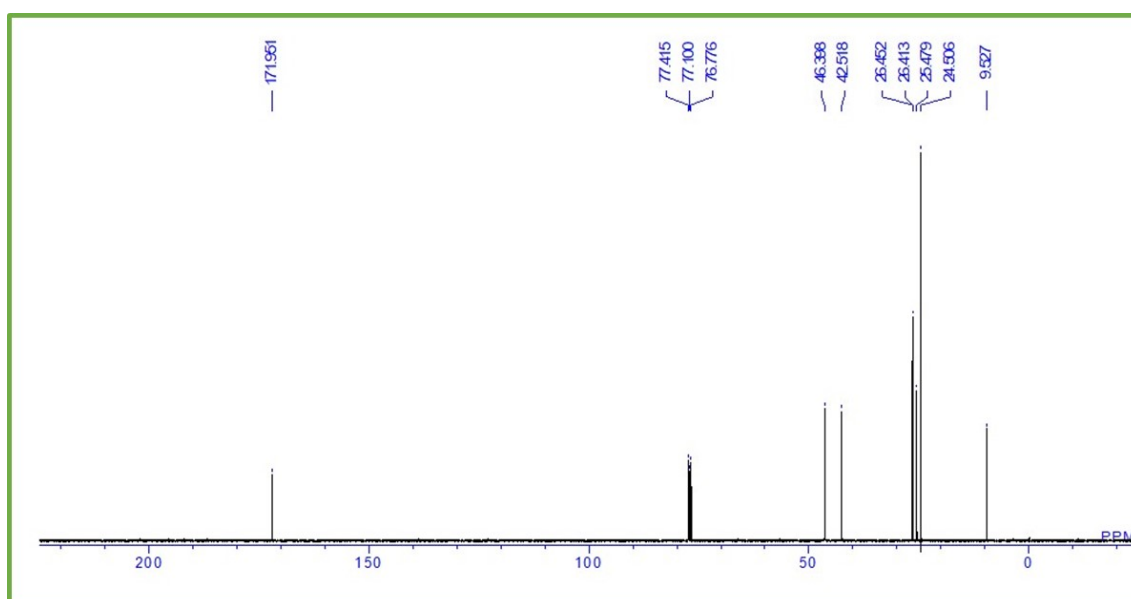
¹³C NMR spectrum of *N*-ethyl 4-piperidone ethylene ketal hydrochloride



***N*-propionylpiperidine**



¹H NMR spectrum of *N*-propionylpiperidine



¹³C NMR spectrum of *N*-propionylpiperidine

7. References

- S1. D. A. Oare, M. A. Henderson, M. A. Sanner and C. H. Heathcock, *J. Org. Chem.*, 1990, **55**, 132–157.
- S2. A. A. N. Magro, G. R. Eastham and D. J. Cole-Hamilton, *Chem. Commun.*, 2007, 3154–3156.
- S3. I. Sorribes, J. R. Cabrero-Antonino, C. Vicent, K. Junge and M. Beller, *J. Am. Chem. Soc.*, 2015, **137**, 13580–13587.
- S4. Y. Shi, P. C. J. Kamer, D. J. Cole-Hamilton, M. Harvie, E. F. Baxter, K. J. C. Lim and P. Pogorzelec, *Chem. Sci.*, 2017, **8**, 6911–6917.
- S5. Y. Shi, P. C. J. Kamer and D. J. Cole-Hamilton, *Green Chem.*, 2017, **19**, 5460–5466.
- S6. T. Toyao, S. M. A. H. Siddiki, Y. Morita, T. Kamachi, A. S. Touchy, W. Onodera, K. Kon, S. Furukawa, H. Ariga, K. Asakura, K. Yoshizawa and K. Shimizu, *Chem. Eur. J.*, 2017, **23**, 14848–14859.
- S7. W. Liu, B. Sahoo, A. Spannenberg, K. Junge and M. Beller, *Angew. Chem. Int. Ed.*, 2018, **57**, 11673–11677.
- S8. B. Emayavaramban, P. Chakraborty and B. Sundararaju, *ChemSusChem*, 2019, **12**, 3089–3093.
- S9. R. Coeck and D. E. De Vos, *Green Chem.*, 2020, **22**, 5105–5114.
- S10. R. Coeck, J. Meeprasert, G. Li, T. Altantzis, S. Bals, E. A. Pidko and D. E. De Vos, *ACS Catal.*, 2021, **11**, 7672–7684.
- S11. W. Rachmady and M. A. Vannice, *J. Catal.*, 2002, **207**, 317–330.
- S12. C. Kaku, S. Sukanuma, K. Nakajima, E. Tsuji and N. Katada, *ChemCatChem*, 2022, **14**, e202200399.
- S13. E. P. Parry, *J. Catal.*, 1963, **2**, 371–379.
- S14. A. A. Bolzan, B. J. Kennedy and C. J. Howard, *Aust. J. Chem.*, 1995, **48**, 1473–1477.